Title
Causal Evidence for Neural Oscillations in Cognition

Author
Riddle, Justin

Publication Date
2018

Peer reviewed|Thesis/dissertation

Causal Evidence for Neural Oscillations in Cognition

By

Justin M Riddle

A dissertation submitted in partial satisfaction of the

requirements for the degree of

Doctor of Philosophy

in

Psychology

in the

Graduate Division

of the

University of California, Berkeley

Committee in charge:

Professor Mark D'Esposito, Chair
Professor Robert Knight
Professor Richard Ivry
Professor Michael Silver

Spring 2018

Abstract

Causal Evidence for Neural Oscillations in Cognition

by

Justin Riddle

Doctor of Philosophy in Psychology

University of California, Berkeley

Professor Mark D'Esposito, Chair

Since early recordings of the human brain, rhythmic electric fields have been observed emanating from regions involved in the specific information processing demands of which the human subject is engaged. Different oscillatory frequencies have been associated with different types of information processing. Neuroscience in the 21st century has seen a revival in research studying the neural basis of oscillatory activity that has deepened our understanding of the complex network level coordination of brain regions. However, causal evidence for the mechanistic role of neural oscillations is sparse, yet provides vital implications for the neural basis of cognition.

The first experiment examines the specific role of beta (15-30 hertz) and gamma (30-50 hertz) frequency oscillations in top-down and bottom-up attention. By applying rhythmic transcranial magnetic stimulation (TMS), the purported cognitive contributions of beta and gamma oscillations are analyzed with respect to a visual search task that varies the level of top-down attention required for optimal performance.

The second experiment examines the specific role of theta (3-8 hertz) and alpha (8-12 hertz) frequency neural oscillations in the reactivation and suppression of working memory representations. Rhythmic TMS in a retro-cued delayed match-to-sample task causally tested previously reported oscillatory neural signatures for their mechanistic contributions to working memory. The degree to which subjects engaged the regions targeted by TMS in functional magnetic resonance imaging (fMRI) predicted the frequency specific effect of rhythmic TMS.

Simultaneous TMS and fMRI offers a unique opportunity to causally test the communication through coherence proposed with neural oscillations. By stimulating a single brain region in multiple frequency bands, the frequency-by-network specific spread of activation can be quantified. Towards this end, the third experiment develops the methodology of concurrent TMS-fMRI with a proof of principle experiment demonstrating the spread of TMS effects through a functional network. In sum, these projects test for the causal role of neural oscillations in cognition and pave the way for future research to study the network level organization of the brain via neural oscillations.

Table of Contents

Acknowledgements

If not for my amazing support team at UC Berkeley, this Ph.D. work would not have been possible. First and foremost, I would like to thank Mark D'Esposito for giving me a chance at graduate school, trusting that my work on neural oscillations would pan out and fit into the grander scheme of D'Espo lab research. Other notable faculty members along my journey: Robert Knight, Richard Ivry, Michael Silver, and David Presti have all inspired me in unique ways. I aspire to join your ranks in the future.

To the rest of the D'Esposito lab, it truly has been a pleasure working with all of you. I am blessed to have participated in such a supportive and collaborative lab. I would like to thank my fellow graduate students: Elizabeth Lorenc, Dan Lurie, Courtney Gallen, Maxwell Bertolero, Jacob Miller, Daniel Toker, and Adam Eichenbaum. I have felt immense comradery with you all.

The post-doctoral fellows in the lab were always available for council and were invaluable in my success. First, I would like to thank Ian Cameron for inviting me into the lab as his personal assistant when I was an undergraduate. This early training was vital to my success later in life and his mentorship inspired me to pursue academia. I would like to especially thank the brain stimulation post-doc crew: Dobromir Rahnev, Derek Nee, Kai Hwang, Taraz Lee, Rob Blumenfeld, and Arielle Tambini. Thanks to Jason Scimeca and Annastasia Kiyonaga for their working memory expertise and to Rob White and Daniella Furman for their knowledge of dopamine and all things basal ganglia. To Regina Lapate, thank you for your advice along the way and for being a source of joy in the lab.

Last, but not least, the post-doc that I have truly had a blast with: David Vogelsang. You have been a friend, colleague, and fellow adventurer in this game we call life.

The secret to my success in graduate school is predominantly owed to the amazing research assistants with which I have been lucky to work. At the top of that list is Dillan Cellier. She has been working with me since her second semester of freshmen year and it has been a great four years. I wish her all the success in the world. Sofia Dhanani was another outstanding research assistant, helping me with projects for her full four years as an undergraduate. Throughout the years I have had many other brilliant assistants: Zoe Franklin, Matt Joerke, Savannah Frisk, Vyoma Shah, Sandhya Kannan, and Alyssa Marusarz.

To my amazing friends: Jeff DeFond, Jacob Anderson, Steven Hoffman, and Tim Rowe. You have made my life exciting and supported me through it all. To my wonderful girlfriend, Hari Simran Khalsa, thank you for being my rock and life partner in this adventure.

To my parents and siblings, you made me the man I am today and I am eternally grateful for our tightknit bonds that defy my physical distance from home.

Chapter 1

INTRODUCTION

Brain cells process information by generating electric signals that trigger chemical release into their synapses with connecting neurons. The traditional view suggests that signals propagates through a neural circuit via these chemical impulses (Yuste, 2015). However, the electric field generated at the time of an action potential produces a not insignificant impact on its surroundings (Buzsáki et al., 2012). The sensitivity of a neuron to incoming chemical signals is crucially dependent on the transmembrane electrical potential that is determined by the extracellular electric field (Buzsáki, 2006). When many neurons activate coherently, the extracellular field constructively interacts and results in an even stronger and far-reaching field. The neocortex is arranged into cortical columns of parallel fibers of excitatory pyramidal cells. This architectural design is particularly effective at coupling the electric activity of neurons. Furthermore, there are regions of the brain that act as rhythmic pattern generators, presumably due to architectural designs of their particular neural circuitry (Wang, 2010).

The electric fields generated by populations of neurons have been demonstrated to not just be a mere epiphenomenon without causal impact (Fröhlich and McCormick, 2010), but these emergent phenomena are systematically generated by the brain in order to mechanistically serve a function. The network level orchestration of information processing in the brain requires information to flow between specific regions (Fries, 2015). Neural oscillations provide a mechanism by which regions can selective establish a communication channel or disengage from distracting regions. Brain regions synchronize their rhythmically fluctuating sensitivity window such that impulses from one region to the other will impinge on the other when that region is maximally sensitive to incoming information. The dynamic interaction of brain regions can be orchestrated by neural oscillations.

Certain rhythms may be characteristic to a specific neural mechanistic generator and therefore more characteristically process a certain type of information (Wang, 2010; Siegel et al., 2012). For example, the role of the hippocampus in memory formation (Lisman and Jensen, 2013) and the role of the NMDA receptor system in establishing new synaptic connections between neurons both have a theta-gamma time signature (Jensen and Lisman, 1996). The hippocampus has a different means of generating theta and gamma time signatures (Buzsáki, 2002) than the neocortex (Jensen and Lisman, 1996), yet the correspondence in these rhythms provides a mechanism by which the broadcasted signals from the hippocampus can be encoded into specific neural pathways in the cerebral cortex during long-term memory consolidation (Sutherland and McNaughton, 2000). Synchronized neural activity provides a crucial mechanism for orchestrated information processing, however, the mechanistic importance of neural oscillations is met with skepticism (Shadlen and Movshon, 1999).

Correlations between neural phenomenon and cognitive processing is not sufficient for establishing the necessity of neural oscillations in brain function. Causal intervention that

specifically targets the oscillatory activity of a brain region is required to establish neural oscillations as playing a crucial role in the information processing of the brain (Herrmann et al., 2016). The specific associations between various cognitive processing and particular oscillatory signatures requires experiments that not only apply frequency specific causal intervention but systematically manipulate cognitive demands as well (Romei et al., 2011; Chanes et al., 2013).

One challenge associated with causal intervention is that the methods of noninvasive brain stimulation in humans suffer from high subject variability (López-Alonso et al., 2014) and sometimes produce contradictory results (Ziemann and Siebner, 2015). Traditional approaches to noninvasive brain stimulation have attempted to categorize the effects of various stimulation protocols as either inhibitory or excitatory (Huang et al., 2005). However, the particular protocols used inevitably differ in their oscillatory characteristics. These differences in stimulation protocols upon considering the frequency domain representation could systematically impact different brain networks (Romei et al., 2016b). As discussed previously, the theta-gamma rhythm is strongly associated with particular molecular mechanism and specific patterns of inter-regional connectivity. Continuous theta burst repetitive transcranial magnetic stimulation (cTB-TMS) was inspired by this theta-gamma rhythmic pattern in hippocampus. cTB-TMS is used as a means of creating a "virtual lesion" in the region of stimulation (Pascual-Leone et al., 2000). However, the effects of cTB-TMS are often not so easily interpretable when compared to other stimulation protocols (Mochizuki et al., 2005). Given the strong association of the theta-gamma code to learning, memory, and perception it is entirely possible that the effects of stimulation are specific to this network (Romei et al., 2016b). If the rhythmic impact of TMS is emphasized the interpretations of previous findings gain a new light. For example, a previous experiment of mine applied cTB-TMS to the human frontal eye fields and concluded that this region was not involved in top-down cognitive control but instead was only involved in bottom-up processes necessary for saccadic eye movement (Cameron et al., 2015). In this experiment, it is possible that cTB-TMS was specific to the bottom-up processing network but spared the top-down cognitive control network that operates within entirely different frequency bands (Michalareas et al., 2016) with which it is also known to be involved.

The first project (**Ch. 2**) tests for the specific role that beta oscillations play in cognitive control and gamma oscillations play in bottom-up information processing. By applying rhythmic TMS in both beta and gamma frequency to the human analog of the frontal eye fields and the superior parietal cortex during a visual search task that varies the demands of top-down attention. I find causal evidence that beta oscillations are specifically involved with top-down attention in both frontal and parietal cortex. The effect of gamma stimulation was specific to the frontal eye fields, most likely due to this region's role in responding to bottom-up visual stimulus via a direct circuit from visual cortex (Schall et al., 1995). Stimulation in beta versus gamma during this task produced different behavioral effect based on the targeted cognitive process.

The second project (**Ch. 3**) focuses on slower oscillations more associated with distributed macroscopic brain networks: theta and alpha frequency. In this project, subjects performed a retro-cued delayed match-to-sample task in which a previous study found task-relevant theta and alpha oscillations (Wallis et al., 2015). Rhythmic TMS during this experiment was explicitly

geared to produce opposite effects from alpha versus theta TMS. As expected, the behavioral benefit or detriment derived from rhythmic TMS was crucially dependent on the frequency of stimulation. This study highlights the relevance of neural oscillations to causal brain intervention. Given the efficacy of brain stimulation for treating depression (Perera et al., 2016), it is crucial that we better understand the particular mechanisms for how our stimulation is impacting cortical function. In particular, this study found opposite effects dependent on the frequency of stimulation. The frequency of stimulation for many brain stimulation studies is not considered. By targeting subject specific intrinsic frequency bands, we can potentially boost the efficacy of noninvasive brain stimulation in clinical populations and reduce subject variability in those that respond positively.

The third project (**Ch. 4**) works towards establishing a methodology for simultaneous neuroimaging and brain stimulation. In order to properly administer therapeutic intervention with noninvasive brain stimulation, it is crucial to understand the neural mechanisms underlying its behavioral and cognitive impact. Concurrent TMS with fMRI offers high spatial resolution for understanding the spread of TMS effects. Given that neural oscillations are thought to coordinate activity between brain regions, rhythmic TMS combined with fMRI is one of the best methods for testing the efficacy of this technique to truly impact the network associated with a particular frequency band. In order to work towards this goal, we first had to establish a coherent methodology for combining TMS with fMRI that avoided the induced signal corruption as best as possible and then addresses and residual artifacts in pre-processing. We provide a proof of concept experiment to demonstrate the effectiveness of this method and pave the way for other labs to replicate our methodology.

Altogether, these projects provide causal evidence for the role of neural oscillations and emphasize the importance of considering the frequency specific effects of brain stimulation. The projects presented in this thesis represent a novel approach to studying brain function that moves beyond simplistic models that treat neural activity as purely excitatory or inhibitory.

Dissertation Outline

- Section 1 – Neural Oscillations
    - Ch. 2: Causal evidence for the role of neuronal oscillations in top-down and bottom-up attention (Riddle et al., submitted)
    - Ch. 3: Selective reactivation or suppression of working memory representations with rhythmic transcranial magnetic stimulation (Riddle et al., in preparation)
- Section 2 – Simultaneous TMS-fMRI
    - Ch. 4: Developing a methodology for concurrent TMS-fMRI: causal evidence for frontal-striatal loops (Riddle et al., in preparation)

%% SECTION 1 %%

NEURAL OSCILLATIONS

Chapter 2

CAUSAL EVIDENCE FOR THE ROLE OF NEURONAL OSCILLATIOSN IN TOP-DOWN AND BOTTOM-UP ATTENTION

2.1 Abstract

Beta and gamma frequency neuronal oscillations have been implicated in top-down and bottom-up attention. In the present study, we used rhythmic transcranial magnetic stimulation (TMS) to modulate ongoing beta and gamma frequency neuronal oscillations in frontal and parietal cortex, while human subjects performed a visual search task that manipulates bottom-up and top-down attention (pop-out and feature search). Gamma frequency TMS to superior precentral sulcus (sPCS) slowed saccadic reaction times during both task conditions that engaged bottom-up attention, and induced a response bias to the contralateral visual field. In contrary, beta frequency TMS to sPCS and intraparietal sulcus (IPS) decreased trial accuracy only during the feature search condition that engaged more top-down attention. Furthermore, beta frequency TMS increased trial errors when the target was in the ipsilateral visual field for the feature search condition. These results indicate that beta frequency TMS to sPCS and IPS disrupted top-down attention, whereas gamma frequency TMS to sPCS disrupted bottom-up, stimulus-driven attention processes. These findings provide causal evidence suggesting beta and gamma oscillations have distinct functional roles for cognition.

2.2 Introduction

Neuronal oscillations are proposed to be a fundamental mechanism that supports a diverse range of neural processes (Canolty and Knight, 2010; Fries, 2015), and oscillations at different frequency bands could contribute to distinct cognitive processes (Siegel et al., 2012). For example, neurophysiology recordings in non-human primates demonstrated that directed coherence of beta frequency oscillations from frontal to parietal cortex mediated top-down attention during a feature search task (Buschman and Miller, 2007), whereas directed coherence of gamma oscillations from parietal to frontal cortex mediated bottom-up, stimulus-driven attention in a pop-out search task. Other non-human primate and human studies have also found evidence suggesting that gamma frequency oscillations carry sensory feed-forward information across the cerebral cortex, whereas feed-back modulatory information is carried in the beta frequency (Bastos et al., 2015; Michalareas et al., 2016). However, neurophysiology recordings can only provide correlational evidence, therefore a causal manipulation is required to validate these correlational findings, and provide evidence that neuronal oscillations are not an epiphenomenon of the underlying neural computation (Buzsáki, 2006; Fröhlich and McCormick, 2010).

Rhythmic transcranial magnetic stimulation (TMS) has been demonstrated to entrain neuronal oscillations in human electroencephalography (EEG) data (Hanslmayr et al., 2014; Albouy et al., 2017), making it a powerful approach to causally manipulate and dissociate the specific roles of neuronal oscillations in different frequency bands (Romei et al., 2010; 2011; Chanes et al., 2013; Quentin et al., 2016). Here, we used rhythmic TMS to modulate ongoing neuronal oscillations in the beta (20 Hz) and gamma (50 Hz) frequency while human subjects performed a visual search task. The task manipulates levels of top-down attention while subjects search for a visual target under two conditions: a pop-out condition that engages less top-down attention, and a feature search condition that engages more top-down attention. Both conditions require bottom-up, stimulus-driven attention to process the presented stimuli. We applied beta and gamma frequency TMS to the right superior precentral sulcus (sPCS) and the right superior intraparietal sulcus (IPS).

Based on previous studies that showed involvement of gamma frequency oscillations in bottom-up, feed-forward, stimulus-driven attention processes (Börgers and Kopell, 2007; Gregoriou et al., 2009; Marshall et al., 2015; Kornblith et al., 2016), we hypothesized that gamma rhythmic TMS would impact performance during both the pop-out and feature search conditions because both conditions required bottom-up attention to process visual stimuli. In contrast, based on the involvement of beta rhythms in top-down attention selection (Buschman and Miller, 2009; Antzoulatos and Miller, 2016; Stanley et al., 2016; Stoll et al., 2016), we hypothesized that beta rhythmic TMS would modulate performance only during the feature search condition that engaged more top-down attention.

While both IPS and sPCS have long been implicated in visual attention (Corbetta and Shulman, 2002), there is no causal evidence specifying how frequency specific coherence or local neuronal oscillations contribute to attention functions in these regions. In the present study, we applied frequency-specific rhythmic TMS to both sPCS and IPS to causally test the functional roles of beta and gamma neural oscillations for bottom-up and top-down attention processes.

2.3 Materials and Methods

After obtaining informed consent according to the guidelines of the Committee for the Protection of Human Subjects at the University of California, Berkeley, seventeen subjects (9 females, ages 18 to 38, mean = 21.3, SD = 4.5) participated in one session of functional magnetic resonance imaging (fMRI) and three sessions of online rhythmic TMS. Eight additional volunteers completed the MRI session but were subsequently dropped from the study due to excessive head motion (n=3) or inability to meet the time commitment of the study (n=5). We further excluded one male subject's data because his behavioral performance was 3 standard deviations away from the group average, leaving 16 subjects in the reported results.

2.3.1 Visual Search Task

The behavioral task used in all four sessions of our experiment was adapted from a previous non-human primate study (Buschman and Miller, 2007) and consisted of 3 epochs (**Figure 2.1a**). In the first epoch, a sample stimulus was presented for 1 second and had two features: color (red, green, or blue) and orientation (60, 105, or 150 degrees). The width of the sample stimulus was 1 visual degree during fMRI scanning, and 2.5 degrees following TMS administration. In the second epoch, the screen went black for a short delay period of 500 milliseconds. Subjects were instructed to maintain fixation for the duration of the sample and delay epochs. Finally, during the response window epoch, a probe of four stimuli appeared at the corners of the screen (2.5 degrees from fixation during fMRI, 7 degrees during TMS). The sample stimulus was always one of the four probe stimuli. Subjects were instructed to perform a saccade and fixate on the probe stimulus that was identical to the sample stimulus, to be fast and accurate, and to respond within the two seconds response window in which the probe was present. The key manipulation in this task was the similarity between the sample stimulus and the three distractor stimuli in the probe. In the pop-out task, the three distracting stimuli were uniform and did not share a common feature with the sample stimulus. The salient difference between the sample stimuli and the distractors was sufficient to allow subjects to successfully perform the task through bottom-up, stimulus-driven attention (Börgers and Kopell, 2007; Fries, 2015). In the feature search task, each distracting stimuli was unique and matched the sample stimulus in either color or orientation. The subject had to withhold a response and search the array for the stimuli that matched the sample stimulus in both features; in this case, bottom-up attention and top-down attention were engaged. A fixation cross was not present during the delay period and probe since previous research has shown that without it the oculomotor system has a lower threshold for generating saccades in reaction to sensory inputs (Reuter-Lorenz et al., 1991). In this way, we were able to increase our sensitivity of detecting TMS effects on trial accuracy.

Between trials, subjects fixated on a centrally presented cross. During the fMRI session, the inter-trial interval (ITI) was selected from an exponential distribution between 3 and 10 seconds to maximize statistical power in the fMRI analysis (Dale, 1999). During the TMS sessions, the ITI was randomly selected to be either 2, 4, or 6 seconds.

Stimuli were presented using a custom script in MATLAB (The MathWorks, Inc., Natick, Massachusetts, Unite States) with the Psychophysics Toolbox extensions version 3. During the MRI session, the screen resolution was 800 x 600 and back-projected by an AVOTEC projector (Stuart, Florida, Unite States) with a 60 Hz refresh rate onto an 8 by 6-inch screen that was 47 inches from the eye. During the three TMS sessions, stimuli were presented on a 13.4 by 10.6-inch liquid crystal display (LCD) monitor presented 29 inches from the eye with 1280 x 1024 resolution and a 60 Hz refresh rate.

Subject responses were measured using eye trackers. During the fMRI session, the subject's eye position was recorded by an Eyelink 1000 Plus Long-Range Mount (SR Research, Mississauga, Ontario, Canada; version 5.0.4 software) that was calibrated before the first run. During TMS sessions, an Eyelink 1000 Plus Desktop Mount with version 5.0.4 software was used to collect saccade data that was calibrated at the start of each block of six runs. Subjects were instructed to press their head to a forehead mount for consistent eye tracking.

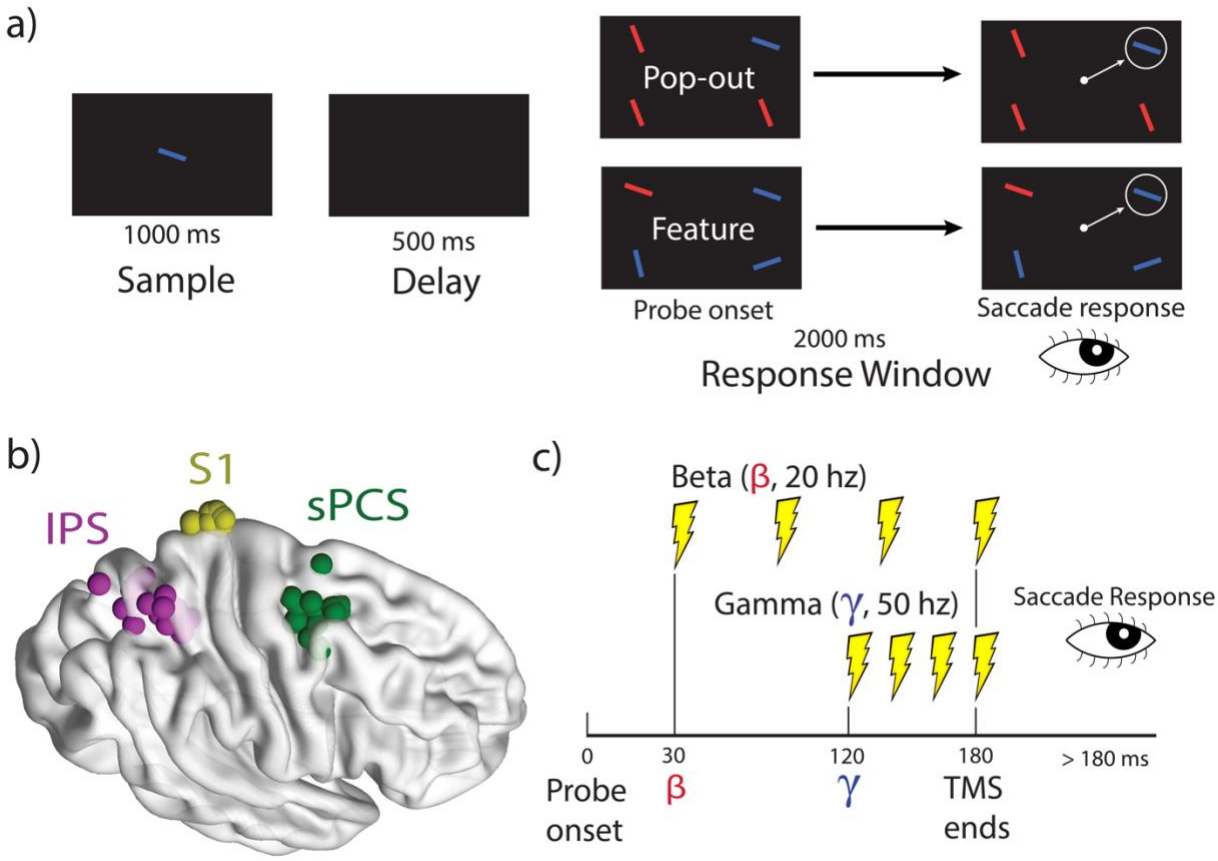

Figure 2.1. Experimental design. (**a**) The visual search task. (**b**) Subject specific regions of interest (ROI) localized by fMRI data and targeted by TMS. (**c**) Timing of rhythmic TMS. Responses were scored based on saccadic RT and trial accuracy. For examples of the criteria used to score an accurate trial see **Figure 2.1-1**.

A custom Matlab script was used for analysis that utilized Eyelink's automated software for saccade detection during acquisition. Subjects were instructed to saccade and fixate on the sample item within the array of probe stimuli and to be "fast and accurate." Each trial was scored for saccadic reaction time (saccadic RT; the time when a saccade was initiated towards a peripheral target) and trial accuracy (correct was defined as a single saccade to the target). Subjects could have had a correct target selection in a trial as indicated by their final fixation, but overtly performed saccades to multiple distractor stimuli before selecting the correct target, therefore rendering the trial accuracy incorrect (**Figure 2.1-1**). Given that gaze may drift without a fixation cross, trials in which the gaze drifted 3-degrees from the center of the screen before presentation of the probe were removed from analysis. On average only 2% of trials with a standard deviation of 1% across subjects were removed because of gaze drift. After the automated eye tracker analysis script was run, experimenters manually checked each trial and corrected any mistakes or failures of the automated analysis.

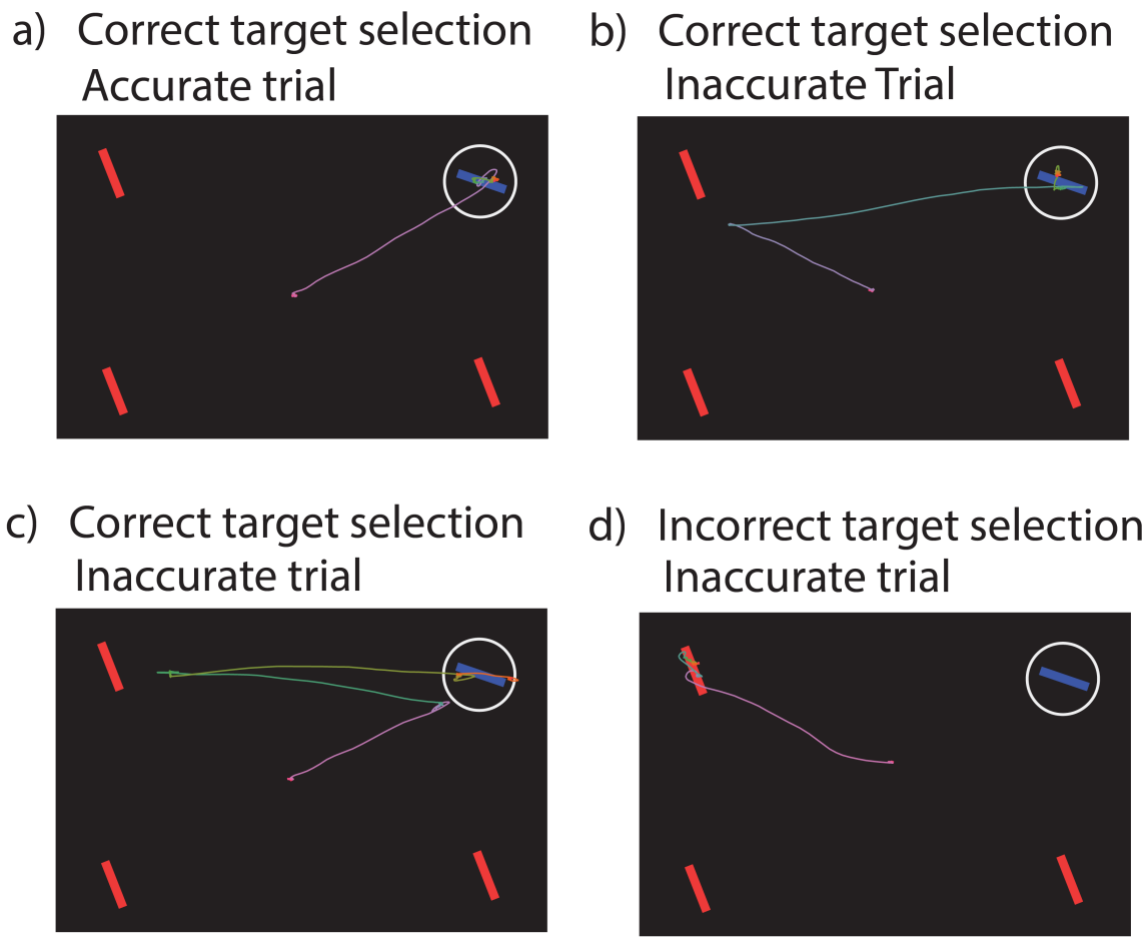

Figure 2.1-1. Trial accuracy criteria. Trials such as (**a**), (**b**), and (**c**) have correct target selection but (**b**) and (**c**) have saccades towards distractor stimuli. Therefore, (**b**), (**c**) and (**d**) were scored as inaccurate trials.

2.3.2 MRI Protocol

During the first session of the experiment, MRI data were collected on a Siemens 3T MAGNETOM Trio (Erlangen, Germany) using a 12-channel receive-only coil at the Henry H. Wheeler, Jr. Brain Imaging Center at the University of California, Berkeley. First, an anatomical image was collected using a T1-weighted magnetization-prepared rapid gradient-echo (MPRAGE) sequence with 192 sagittal slices each 1 mm isotropic voxels, 50% distance between slices (0.5 mm), 2.3 second repetition time, interleaved slice acquisition, phase-encoding direction from anterior to posterior, 2.98 millisecond echo time, 9-degree flip angle, and parallel imaging via GeneRalized Autocalibrating Partial Parallel Acquisition (GRAPPA) with an acceleration factor of 2. Next, functional data were collected during performance of the visual search task using a T2*-weighted single-shot echo-planar imaging (EPI) sequence with 37 slices each 3.5 mm isotropic voxels, 20% distance between slices (0.7 mm), 2 second repetition time, descending slice acquisition, phase encoding direction anterior to posterior, 24 millisecond echo time, 60-degree flip angle, fat

saturation, and prescan normalization. The first 2 volumes of every functional run were discarded upon acquisition; and for analysis purposes, the first two recorded volumes were also discarded.

Preprocessing of fMRI data was performed using the Statistical Parametric Mapping 12 toolbox (SPM12, www.fil.ion.ucl.ac.uk/spm) in MATLAB (version 2014a release). All preprocessing steps were performed in SPM12 unless otherwise noted. The anatomical image had the neck removed (AFNI, (Cox, 1996)), manual reorientation to the anterior commissure, segmentation with mean bias correction, and skull stripping (FSL 4.1.9, fsl.fmrib.ox.ac.uk/fsl/). The functional data were de-spiked at 3 standard deviations above the mean (AFNI, (Cox, 1996)), slice time corrected, rigid body motion aligned to the mean functional image, manually reoriented to the anterior commissure, and smoothed with a FWHM kernel of 4 millimeters.

2.3.4 Region of Interest Localization

After the first session, a univariate analysis of the fMRI data was performed in each subject's native space with a general linear model analysis that included 8 nuisance regressors: 6 rigid body motion realignment parameters and the mean signal in white matter (WM) and cerebral spinal fluid (CSF). The masks for WM and CSF were calculated by SPM12's segmentation of the anatomical image. Each trial was modeled as an event with onset at the start of the target epoch and duration until the saccadic RT. If no saccade was made, then the event duration included the full 2 second response window. The onset and duration of these events was convolved with the canonical hemodynamic response function and 5 task regressors were generated: correct and incorrect feature-search and pop-out, and miss trials.

The activation map for all correct trials was used to identify regions of interest (ROIs) for targeting with TMS in sessions 2, 3, and 4. The subject specific ROIs were normalized into the Montreal Neurological Institute's standardized space for display purposes (**Figure 2.1b**). The right sPCS ROI was defined as the peak contrast value at the intersection of the precentral sulcus and superior frontal sulcus. The coordinates of the average sPCS ROI in MNI space after normalization was x = 27 mm, y = 0 mm, z = 57 mm with standard deviation of x = 5 mm, y = 5 mm, z = 6 mm. sPCS is the human analog of the frontal eye fields (FEF) typically defined as the region at which electrical stimulation of neurons resulted in contralateral eye movements (Robinson and Fuchs, 1969). sPCS has contralateral visual field maps and plays a prominent role in saccadic eye movements to the periphery, but may play a more extensive role in humans for its involvement in attention and cognitive control (Vernet et al., 2014).

The right superior IPS ROI was defined as the peak activation in the dorsal region of the IPS. The coordinates of the average IPS ROI in MNI space after normalization was x = 29 mm, y = -56 mm, z = 56 mm with standard deviation of x = 7 mm, y = 9 mm, z = 6 mm. Previous fMRI studies on visual search have found the same superior IPS region involved in conjunctive feature search greater than single feature search (Donner et al., 2002; Shulman, 2003). The homologous region in monkeys, the lateral intraparietal area, displays a few idiosyncratic differences from the human

site but is considered most equivalent in anatomy and function to the medial superior IPS site in humans (Grefkes and Fink, 2005) that was targeted in this experiment.

The right primary sensory cortex (S1) ROI was defined as the dorsal medial region of the post central gyrus and roughly corresponds to sensory input from the legs. No significant task-related modulation was found in the S1 ROI during fMRI across subjects. The coordinates of the average S1 ROI in MNI space was x = 8 mm, y = -39 mm, z = 79 mm with standard deviation of x = 1 mm, y = 3 mm, z = 2 mm. S1 was used as a control stimulation site to account for non-specific TMS effects. This site has been demonstrated to be an effective control site for TMS stimulation of the oculomotor network given its close proximity to the oculomotor network and its inactivity during saccadic tasks (Cameron et al., 2015). The average distances between TMS target sites were: sPCS and IPS, 57 mm; IPS and S1, 38 mm; and sPCS and S1, 49 mm. The spatial resolution of TMS has previously been demonstrated as sufficient to dissociate ROIs with this distance (Wagner et al., 2009a).

2.3.5 Transcranial Magnetic Stimulation

During sessions 2, 3, and 4 of the experiment, TMS was delivered using a MagStim Super Rapid-2 Plus1 stimulator with a figure-eight 70mm double air film coil (MagStim, Whitland, United Kingdom). Each subject's motor threshold (MT) was calculated to calibrate the coil intensity to their specific sensitivity level. To calculate a subject's MT, an electrode was attached to the first dorsal interosseous muscle on the left hand of the subject. Single pulses of TMS were delivered to the corresponding hand region of the motor cortex at a 45 degree angle until the TMS pulses reliably elicited a motor evoked potential (MEP), defined as a near instantaneous voltage increase of at least 70 microvolts above baseline (O'Shea et al., 2007). Once an MEP was generated, the intensity was decreased to a level that elicited an MEP on 5 out of 10 pulses.

To trigger the TMS coil during online TMS, a custom built serial cable triggered trains of 4 biphasic pulses with an inter-pulse interval of either 20 or 50 Hz (beta or gamma frequency) at high or low (110% or 50% of MT) coil output. The low intensity TMS was beneath the threshold for modulating neuronal activity, therefore we hypothesized that high intensity TMS would result in stronger behavioral modulation compared to low intensity TMS. During online TMS, subjects were actively monitored for signs of duress and were encouraged to inform the experimenter of any discomfort. For one subject, TMS to sPCS elicited muscle twitching and the TMS amplitude was lowered by 5% to reduce head movement.

To ensure the accuracy of TMS targeting, we used Rogue Research's BrainSight v2.2.11 (Rogue Research, Montreal, Canada) with a Northern Digital Polaris Spectra infrared camera (Waterloo, Ontario, Canada) to register coordinates around the subject's head to their anatomical MRI scans with stereotaxic 3-dimensional tracking. Subject specific ROIs derived from the fMRI data were overlaid on the subject's anatomical image and a trajectory for TMS was calculated to be perpendicular to the skull. The coil angle was held constant in the posterior to anterior direction for all three ROIs. During the TMS sessions, experimenters actively maintained a stable position

of the TMS coil aided by a MagStim coil holder and continuous stereotaxic tracking. We maintained the TMS coil position to be under 5 millimeters and 5 degrees of error.

A previous non-human primate neurophysiology study with a similar visual search task demonstrated that upon presentation of the probe, the identity of the target stimulus could be decoded from spiking activity in frontal and parietal cortex (Buschman and Miller, 2007). Decoder accuracy accumulated in the 200 milliseconds prior to the saccadic reaction time and also coincided with coherence effects in beta and gamma frequency oscillations (Buschman and Miller, 2007). Based on these findings, in the current experiment, rhythmic TMS was delivered such that the 4-pulse train ended at 180 milliseconds after the presentation of the probe (**Figure 2.1c**). Crucially, the timing of rhythmic TMS was chosen to maximally align frequency specific stimulation to coincide with the coherence effect previously reported. Thus, beta frequency TMS started 30 milliseconds after the onset of the probe and gamma frequency started 120 milliseconds after the onset of the probe.

During each session of online rhythmic TMS, subjects completed one block of beta frequency TMS at 20 Hz and one block of gamma frequency TMS at 50 Hz in counterbalanced order across subjects. Subjects were given a minimum of a ten-minute break between the two blocks. Each block consisted of 6 runs of 32 trials each with a short self-paced break between each run. Within each run, there were two task conditions (pop-out or feature search) and two TMS intensity conditions (110% or 50% of motor threshold), which were randomized and counterbalanced. Overall, subjects completed 384 trials on each TMS day with 48 trials in each experimental condition. After removal of trials in which the subject broke fixation or performed a saccade before the completion of TMS, the average number of trials per condition was 34.5 (38.9 median) with a standard deviation of 10.4.

2.3.6 Statistical analysis

The frequency specific effects of TMS on subject performance was assessed based on saccadic RT for trials in which the subject correctly identified the target in the probe, as well as trial accuracy. We hypothesized that TMS would have a frequency specific impact. Gamma frequency TMS should impact behavioral performance during both the pop-out and feature search tasks (both employed bottom-up attention) while beta frequency TMS should impact behavioral performance only during the feature search task (top-down attention was required). Based on this prediction, we performed two repeated-measures Analysis of Variance (ANOVA) using RT and trial accuracy as dependent variables, and Task condition (pop out versus feature search), TMS intensity (high versus low), TMS frequency (beta versus gamma), and TMS site (sPCS and IPS) as independent variables. Given our focus on beta and gamma frequency oscillations, we tested for a main effect of TMS frequency or an interaction of frequency with other experimental factors. After identifying significant main or interaction effects, we performed follow-up post-hoc t-tests while controlling for multiple comparisons using Tukey's correction procedure.

To control for non-specific physiologic effects of rhythmic TMS such as auditory entrainment and the general effect of noninvasive brain stimulation to the brain, all analyses are reported as the difference in performance following TMS to sPCS or IPS compared to condition matched TMS to the control site. Furthermore, we expected that low intensity TMS should have no or weaker impact on behavioral performance compared to high intensity TMS, given that TMS was delivered below the motor threshold required to elicit overt motor behavior.

Receptive fields in sPCS and IPS are lateralized to represent the contralateral visual field (Silver and Kastner, 2009), and previous research found that gamma frequency TMS to sPCS resulted in an increase in reporting the detection of a low contrast stimulus in the contralateral visual field even when the stimulus was not present, essentially creating a phantom bottom-up signal (Chanes et al., 2013). Therefore, gamma frequency TMS to sPCS could systematically bias subjects to saccade to the contralateral visual field. Given that TMS was applied to the right hemisphere, we calculated response bias as the number of error trials with the first saccade toward the left visual field divided by the total number of error trials. Note that the probability of stimuli presented in each visual field was 50%.

Previous research on beta frequency rhythmic TMS to sPCS found an increase in d-prime, a metric of successful signal detection, in the contralateral visual field (Chanes et al., 2013). Thus, we hypothesized that beta frequency TMS would modulate top-down attention signals towards the contralateral visual field resulting in a search bias. We calculated search bias as the number of error trials with the target in the ipsilateral visual field divided by the total number of error trials. For example, a search bias towards the contralateral visual field means there were more saccade errors when the target was in the ipsilateral visual field.

2.4 Results

Our experiment was designed to test for frequency specific effects of beta versus gamma frequency TMS on saccadic RT and trial accuracy. We predicted an effect of high intensity gamma frequency TMS on both pop-out and feature search conditions given that both conditions employed bottom-up attention. We also predicted an interaction of high intensity beta frequency TMS and task condition given that the feature search condition likely engaged more top-down attention. Given that receptive fields in sPCS and IPS are lateralized to represent the contralateral visual field (Silver and Kastner, 2009), we predicted that high intensity gamma frequency TMS would lead to a contralateral response bias and high intensity beta frequency TMS would lead to a contralateral search bias. We tested these predictions with ANOVA and post-hoc statistical tests.

2.4.1 Task Effects: Saccadic Reaction Time

We first performed a four-way (Task condition x TMS intensity x TMS frequency x TMS site) repeated-measures ANOVA for saccadic RT (mean of 230 milliseconds and standard deviation of

30 across all conditions). We predicted a main effect of TMS frequency or an interaction of TMS frequency with the other experimental factors. Consistent with our predictions, we found a main effect of TMS frequency ($F(1,15) = 4.78$, $p = 0.045$, $\eta^2_p = .24$) and an interaction between TMS frequency x TMS site ($F(1,15) = 7.38$, $p = 0.0159$, $\eta^2_p = .33$). The interaction of TMS frequency by TMS site suggested that gamma and beta frequency TMS induced different effects when applied to IPS and sPCS. Therefore, we separately compared the effect of beta versus gamma frequency TMS in sPCS and IPS using post hoc tests, while controlling for multiple comparisons using the Tukey procedure. We found a significant difference between gamma and beta frequency TMS in sPCS ($t(15) = 3.58$, Tukey adjusted $p = 0.01$, $d = 0.87$), but no difference between gamma and beta frequency TMS in IPS ($t(15) = 1.054$, Tukey adjusted $p = 0.72$, $d = 0.29$). This effect was driven by a slowing of saccadic RTs following gamma frequency TMS relative to control TMS ($t(15) = 3.14$, Tukey adjusted $p = 0.0063$, $d = 0.56$; **Figure 2.2a**), whereas beta frequency TMS to sPCS had no effect on saccadic RT ($t(15) = -0.65$, Tukey's adjusted $p = 0.77$, $d = 0.24$; **Figure 2.2a**). All conditions for saccadic RT are displayed in the Extended Figures (**Figure 2.2-1, 2.2-2**). Consistent with our hypothesis that gamma frequency oscillations would impact bottom-up attention, our results demonstrated that gamma frequency TMS to sPCS increased saccadic RT during both the pop-out and feature search tasks. We also found that gamma frequency TMS to sPCS slowed saccadic RT irrespective of TMS intensity.

Given the lateralized receptive field in sPCS, we predicted that gamma frequency TMS to the right sPCS will cause a response bias towards the contralateral left visual field. To test this hypothesis, we analyzed the direction of the first saccade for all error trials during the feature search task following high intensity TMS (there were not enough errors in the pop-out task to include task as a factor in the analysis). A two-way repeated-measures ANOVA (TMS frequency x TMS site) showed a main effect of TMS frequency ($F(1,15) = 5.69$, $p = 0.031$, $\eta^2_p = .28$; **Figure 2.2b**). Post-hoc tests revealed increased erroneous saccades to the contralateral side (response bias) from gamma frequency TMS to sPCS ($t(15) = 2.51$, Tukey adjusted $p = 0.030$, $d = 0.59$), but not from beta frequency TMS ($t(15) = -0.676$, Tukey adjusted $p = 0.75$, $d = 0.0095$). Neither beta, nor gamma, frequency TMS to the control site caused a response bias.

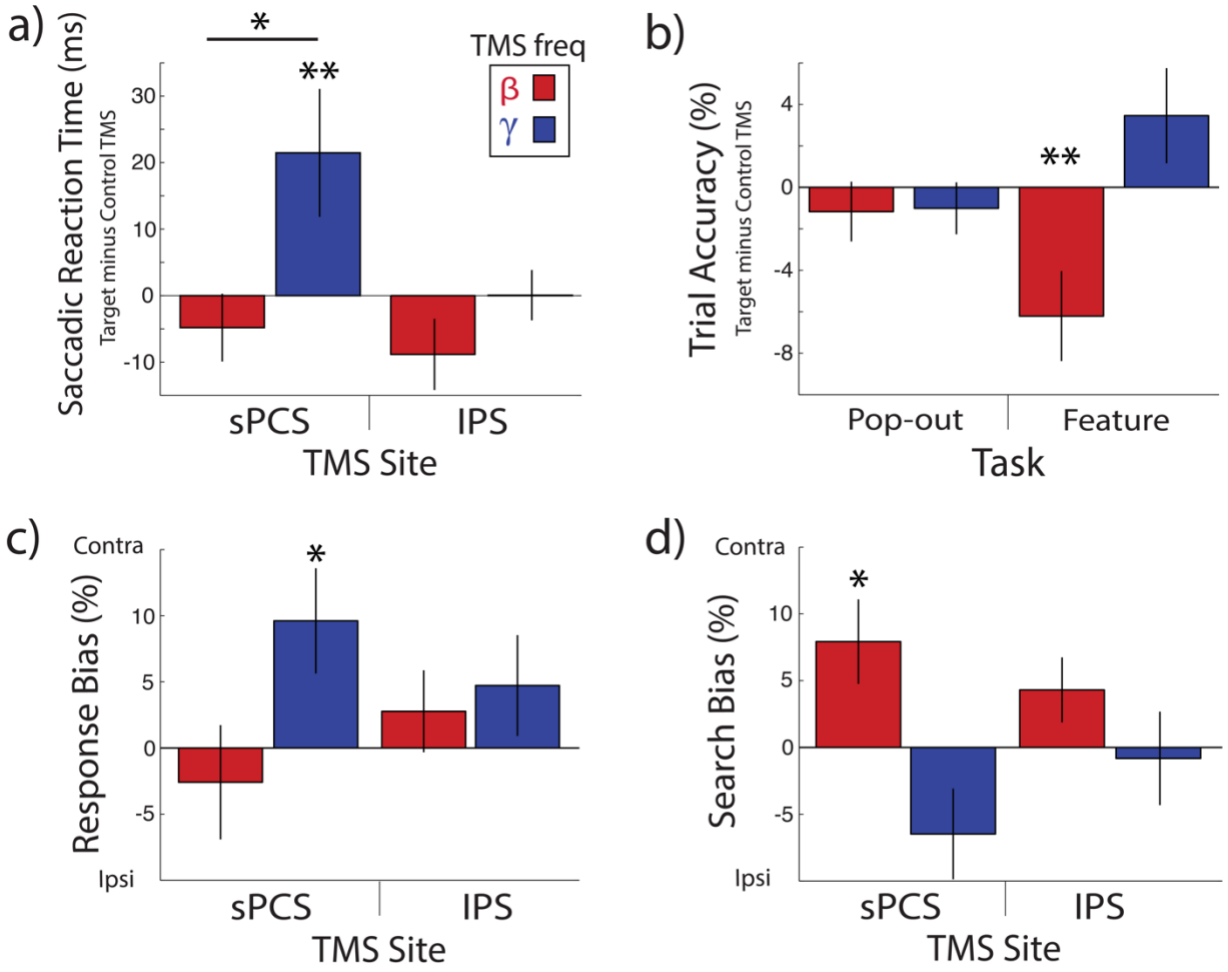

Figure 2.2. Frequency specific TMS effects on behavior. (**a**) 4-way ANOVA of saccadic RT revealed an interaction between TMS frequency and TMS site. (**b**) 3-way ANOVA of trial accuracy for high intensity TMS revealed an interaction between TMS frequency and Task. (**c**, **d**) Analysis of feature search error trials during high intensity TMS. (**c**) 2-way ANOVA of response bias revealed a main effect of TMS frequency. (**d**) 2-way ANOVA of search bias revealed a main effect of TMS frequency. Error bars display the standard error to the mean; * Tukey's adjusted $p < 0.05$; ** Tukey's adjusted $p < 0.01$. All behavioral data is displayed in **Figure 2.2-1** and **Figure 2.2-2**.

2.4.2 Task Effects: Trial Accuracy

We further tested how frequency-specific TMS would impact trial accuracy. We performed a four-way (Task x TMS intensity x TMS frequency x TMS site) repeated-measures ANOVA on trial accuracy (mean of 71% and standard deviation of 8% across all conditions) to test for a main effect or interaction with TMS frequency. This analysis revealed a significant TMS frequency x TMS intensity interaction ($F(1,15) = 7.72$, $p = 0.014$, $\eta^2_p = .34$), suggesting that high versus low intensity TMS had differential effects on trial accuracy. To determine those differential effects,

we performed two three-way repeated-measures ANOVA (Task x TMS frequency x TMS site) separately on low and high TMS intensity conditions, and found that low intensity TMS did not induce any significant effect on trial accuracy. However, the high intensity TMS had a significant main effect of TMS frequency ($F(1,15) = 8.97$, $p = 0.0091$, $\eta^2_p = .37$) and a significant interaction between TMS frequency and Task ($F(1,15) = 4.81$, $p = 0.044$, $\eta^2_p = .24$; **Figure 2.2c**). This interaction effect suggested that rhythmic TMS had different effects on trial accuracy for the feature search versus the pop-out search task. Specifically, we found that compared to control TMS, only beta frequency TMS impaired trial accuracy during the feature search task ($t(15) = -3.176$, Tukey adjusted $p = 0.0038$, $d = 0.72$), but not gamma frequency TMS ($t(15) = 1.64$, Tukey adjusted $p = 0.196$, $d = 0.38$). All conditions for trial accuracy are displayed in the Extended Figures (**Figure 2.2-1,2.2-2**). These findings support our hypothesis that beta frequency TMS would selectively impact the feature search condition that required top-down attention, and would not impact the pop-out that requires less top-down attention.

Given the lateralized receptive fields in sPCS and IPS, beta frequency TMS could lead to a feature search bias towards a specific visual field. Thus, we predicted that beta frequency TMS would induce a search bias towards the contralateral visual field, such that there were increased errors when the target was in the ipsilateral relative to the contralateral visual field. We preformed two-way repeated-measures ANOVA (TMS frequency x TMS site) on error trials for the high intensity TMS feature search condition. We found a main effect of TMS frequency ($F(1,15) = 12.7$, $p = 0.0029$, $\eta^2_p = .46$; **Figure 2.2d**). In line with our hypothesis, we found that a search bias was induced towards the contralateral visual field for beta ($t(15) = 2.586$, Tukey adjusted $p = 0.03$, $d = 0.81$), but not gamma ($t(15) = -1.545$, Tukey adjusted $p = 0.24$, $d = -0.34$), frequency TMS. Neither beta, nor gamma, frequency TMS to the control site caused a search bias.

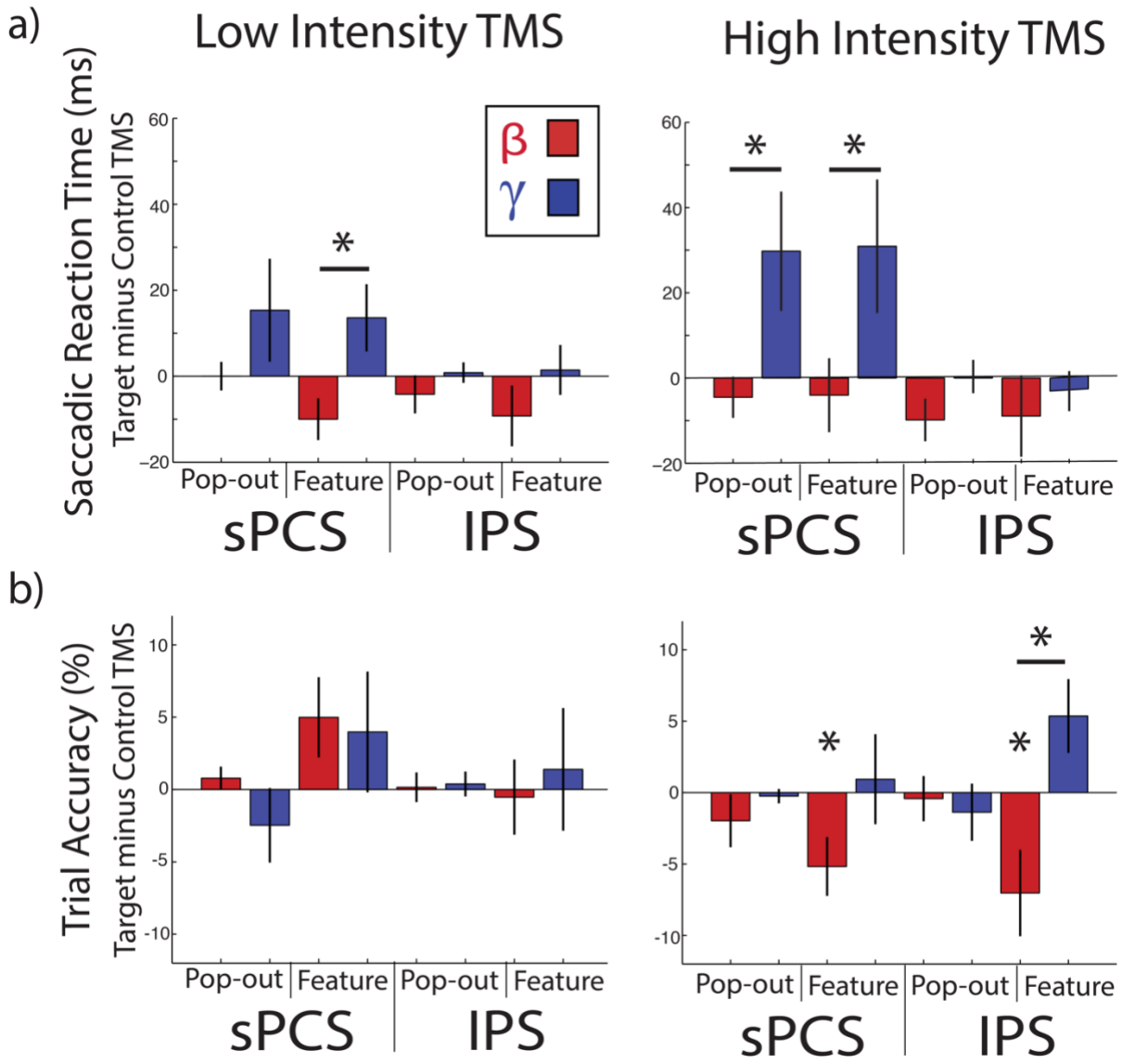

Figure 2.2-1. Behavioral effect of rhythmic TMS minus control TMS for (**a**) saccadic RT and (**b**) trial accuracy at low and high intensity TMS. Error bars display the standard error to the mean. * $p < 0.05$, uncorrected.

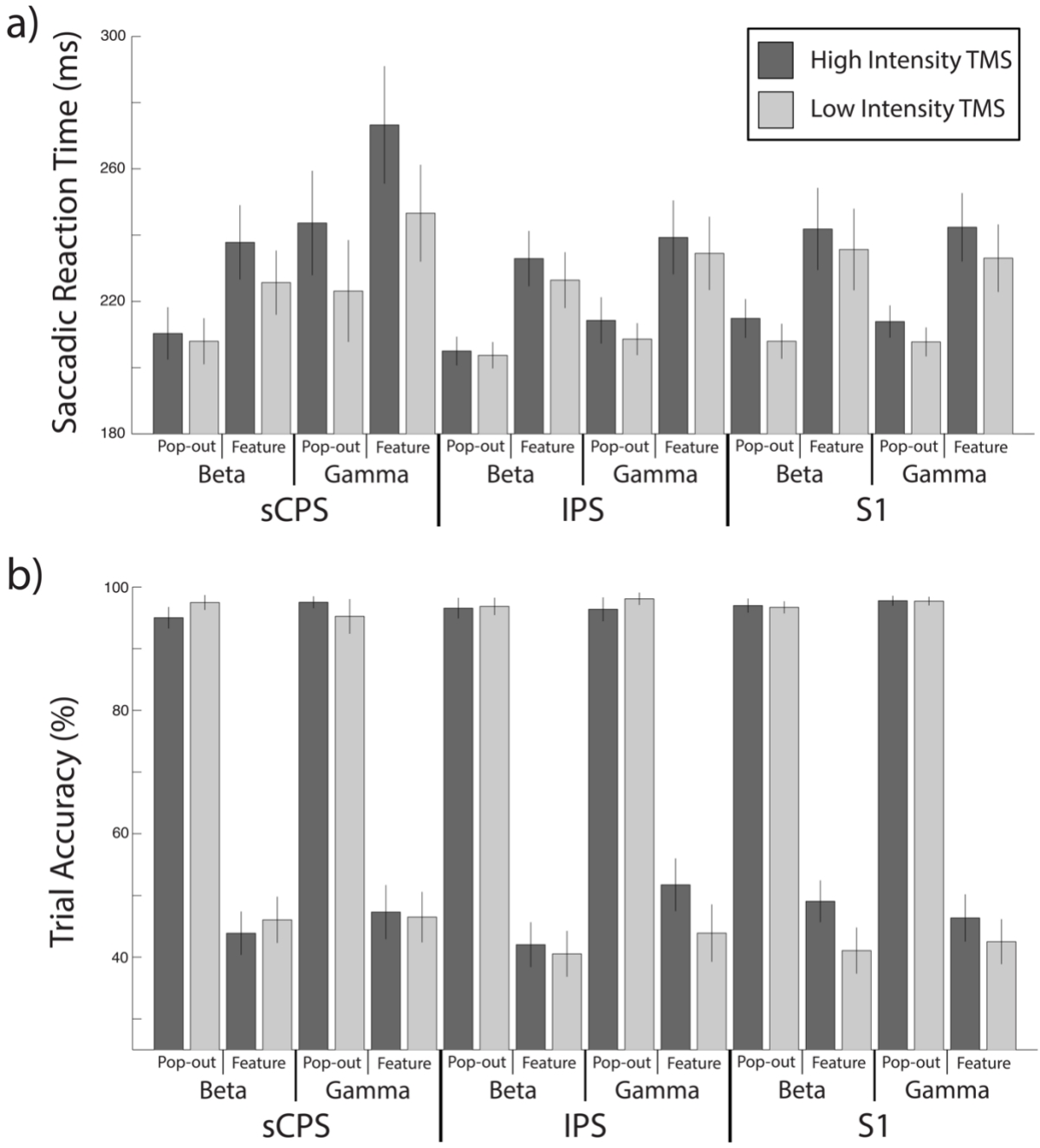

Figure 2.2-2. All behavioral conditions for (**a**) saccadic RT and (**b**) trial accuracy. Error bars display the standard error to the mean.

2.5 Discussion

Our results demonstrated that rhythmic TMS at specific frequencies can modulate specific cognitive processes. Moreover, these findings provide causal evidence supporting the proposal

that top-down attention is mediated by beta frequency neuronal oscillations, whereas bottom-up attention is mediated by gamma frequency neuronal oscillations (Buschman and Miller, 2007). Specifically, we found that gamma frequency TMS to sPCS slowed saccadic RTs during both pop-out and feature search conditions, both of which required bottom-up attention. Furthermore, we found that gamma frequency TMS to sPCS increased response bias to the contralateral visual field. Consistent with our findings, a previous study found that gamma, but not beta frequency TMS to sPCS produced a bias towards reporting a low contrast stimulus in the contralateral visual field even if it was not present, perhaps due to a phantom bottom-up signal induced gamma frequency TMS induced (Chanes et al., 2013). Direct projections from visual areas, such as V4, to sPCS (Schall et al., 1995) form a bottom-up pathway for stimulus driven visual information, and this pathway exhibits increased inter-areal coherence in the gamma frequency during attention (Gregoriou et al., 2009). sPCS also has direct projections to the superior colliculus, and direct stimulation in animals elicit saccadic eye movements (Robinson and Fuchs, 1969). Given this network organization, gamma frequency TMS to sPCS may have disrupted gamma coherence between early visual regions and sPCS, which disrupted processing of salient visual stimuli, resulting in slower saccadic RTs. Slower saccadic RTs could reflect diminished transmission of bottom-up excitatory visual input from visual cortex to sPCS that is necessary to guide saccade generation in both tasks.

Alternatively, gamma frequency TMS to sPCS may have impacted local gamma frequency neuronal oscillations, and induced a signal that mimicked bottom-up signals from visual cortex. The induced local gamma frequency neuronal oscillations could have driven bottom-up attention towards the contralateral visual field, resulting in a response bias towards the contralateral visual field. The communication through coherence hypothesis suggests that gamma frequency oscillations modulate excitation-inhibition balance for bottom-up attention selection (Fries, 2015). In this model, excitatory activity within a neural circuit triggered by sensory input can be dampened by local inhibitory interneurons, resulting in an inactivation period that lasts roughly the duration of a gamma cycle (Börgers and Kopell, 2007). As the inactivation period expires, the neural circuit becomes ready for a new volley of excitatory input. Therefore, a neural circuit can be more sensitive to excitatory input timed to the gamma frequency range (Börgers and Kopell, 2007). In our study, the first gamma frequency TMS pulse could have triggered neural firing and a subsequent local inhibition. As the inhibition relaxed, the next TMS pulse could have been timed to maximally reactivate the circuit. Thus, our repeated pulses of gamma frequency TMS to the sPCS could have driven the excitatory bottom-up signaling pathway that is usually triggered in response to contralateral visual stimuli transmitted from the visual cortex. In this way, gamma frequency TMS could mimic the activity of a salient stimuli in the contralateral visual field, leading to a saccade.

Consistent with previous neurophysiology studies that showed beta coherence between sPCS and IPS during top-down attention (Buschman and Miller, 2007), we found that beta, but not gamma frequency TMS, disrupted trial accuracy when applied to both sPCS and IPS during the feature search condition. Since the effect of beta frequency TMS on trial accuracy was similar when applied to both sPCS and IPS, this finding suggests that beta coherence between sPCS and IPS was necessary for top-down attention. Beta-band oscillations are common during a variety

of tasks that require superposing a task-goal over stimulus driven activity (Engel and Fries, 2010). For example, during the delay period of a delayed matched-to-sample task, FEF and prefrontal cortex ventral to the principal sulcus in non-human primates exhibited an increase in beta oscillatory bursts that track the top-down maintenance of a stimulus representation (Lundqvist et al., 2016). Also, when making categorical judgments about presented stimuli, coherent beta frequency oscillations between regions of parietal and frontal cortex increased stimulus-driven gamma frequency oscillations in regions that represent task-relevant information over regions processing irrelevant information (Antzoulatos and Miller, 2016). Consistent with these findings, we found that beta frequency TMS modulated top-down attention processes when delivered to both sPCS and IPS.

We further found that when beta frequency TMS was applied to sPCS and IPS during the feature search condition, subjects made more errors when the target was in the ipsilateral visual field. A previous study demonstrated that beta frequency oscillations during a similar feature search task tracked the shift of a single spotlight of attention through each item within a probe array of four different stimuli (Buschman and Miller, 2009). Thus, our findings could indicate that beta frequency TMS caused a search bias towards the contralateral visual field through exogenously entrained beta oscillations, at the expense of searching the receptive fields of the ipsilateral side. Our results are further consistent with a previous study that found that only beta, not gamma, frequency TMS to sPCS increased perceptual sensitivity, potentially through enhanced top-down signaling to the contralateral visual field (Chanes et al., 2013).

Previous studies found that coherent beta oscillations between frontal and parietal regions modulate gamma oscillations to sharpen gain (Stanley et al., 2016), bias gamma activity towards processing relevant categories (Antzoulatos and Miller, 2014), and boost gamma activity corresponding to active stimulus processing (Richter et al., 2017). Layer-specific recordings demonstrated that beta oscillations expressed more strongly in the deep layers while gamma activity was stronger in the superficial layers (Bastos et al., 2018), and that beta oscillations in deep layers act to modulate the superficial layers (Bastos et al., 2018). Given that our results showed that rhythmic TMS to a single cortical region in beta versus gamma frequency have different effects on behavior, rhythmic TMS could have causally modulated specific layers of cortex and their associated top-down and bottom-up signaling pathways.

In summary, we found that rhythmic TMS delivered in different frequencies to a brain region can result in different behavioral effects. This suggests that the behavioral and cognitive processes can be dissociated not only by the location of brain regions, but also by frequency bands that carry relevant functional signals. The efficacy of TMS can therefore be improved by targeting the endogenous oscillatory activity of a brain region or a particular cognitive function. Our findings indicate that beta and gamma frequency neuronal oscillations underlie top-down and bottom-up attention, respectively, and that rhythmic TMS can modulate their associated cognitive process.

Chapter 3

SELECTIVE REACTIVATION OR SUPPRESSION OF WORKING MEMORY REPRESENTATIONS USING RHYTHMIC TRANSCRANIAL MAGNETIC STIMULATION

3.1 Abstract

Causal manipulation is required to validate the mechanistic role of neural oscillations in cognitive processing. Noninvasive brain stimulation studies often suffer from high subject variability and stimulation can result in benefits or detriments to performance. To resolve this confusion, we propose that the effect of brain stimulation depends on the ongoing task-relevant oscillatory activity in the targeted region. Here, we use a retrospective-cue working memory (WM) task designed to drive task-relevant alpha and theta oscillations in parietal and prefrontal cortex, respectively. To causally test our hypothesis, we applied rhythmic transcranial magnetic stimulation (TMS) in either alpha or theta frequency to prefrontal and parietal sites. In support of our hypothesis, we found an interaction such that the effect of rhythmic TMS on WM performance was dependent on whether the TMS frequency matched the task-relevant oscillatory activity of the targeted region. These results causally establish dissociable roles for parietal alpha and prefrontal theta oscillations in WM and demonstrate how the effect of TMS can depend on the nature of ongoing processing and task-relevant oscillations in the targeted region.

3.2 Introduction

Neural oscillations are predictive of the information processing occurring within the human brain and may provide a mechanism of information transfer (Fries, 2015), selective communication (Fries et al., 2001), and the binding of representations (Lisman and Jensen, 2013). Noninvasive brain stimulation offers a powerful tool for establishing a causal connection between the oscillations occurring at the mesoscopic scale and their mechanistic role in cognitive functions (Thut, 2011). However, noninvasive brain stimulation has been known to exhibit high inter-subject variability (López-Alonso et al., 2014) and often produces weak findings that can be contradictory between experiments (Ziemann and Siebner, 2015). We propose that the efficacy of transcranial magnetic stimulation (TMS) is crucially dependent on the cognitive processing and corresponding task-relevant endogenous oscillatory activity of the stimulated region at the time of stimulation. Here we use rhythmic TMS to test this prediction in the context of working memory (WM).

To systematically drive endogenous activity, we draw on previous work demonstrating that working memory has key neural oscillatory signatures in alpha and theta frequency (Klimesch et al., 1997; Roux and Uhlhaas, 2014; Wallis et al., 2015). When visual stimuli are presented in both the left and right visual hemifields and a preceding cue indicates that one hemifield should be

prioritized for encoding into WM, there is an increase in alpha oscillatory activity in occipito-parietal cortex ipsilateral to the prioritized hemifield (Klimesch, 2012). This signature alpha activity has been functionally linked to a selective attention mechanism that proactively suppresses cortical processing of the stimuli presented in the irrelevant visual hemifield (Sauseng et al., 2009; Klimesch, 2012). Selective attention can also operate on internally maintained WM representations (Griffin and Nobre, 2003; Gazzaley and Nobre, 2012), and alpha activity has recently been linked to the suppression of task-irrelevant WM representations: when a retrospective cue (retro-cue; (Souza and Oberauer, 2016)) is presented during the delay period to indicate which memoranda are task-relevant, this drives a similar pattern of alpha activity in occipito-parietal cortex (Poch et al., 2014; Wallis et al., 2015; Poch et al., 2017; 2018). Resilience to distraction and interference is a hallmark of WM performance, and selective attention is therefore critical to maintain target information throughout a delay period (Gazzaley and Nobre, 2012; D'Esposito and Postle, 2015); when a subset of WM representations is no longer relevant, alpha oscillations could be the means by which the now irrelevant representations are inhibited (Jokisch and Jensen, 2007; Crespo-Garcia et al., 2013). For the proactive suppression of irrelevant information, alpha oscillations in parietal cortex have been causally established as a mechanism of suppressing irrelevant visual stimuli (Sauseng et al., 2009); however, the suppression of irrelevant representations within WM via alpha oscillations has not yet been causally established.

Complimentary to the inhibitory role of alpha oscillations, theta oscillatory activity emerges particularly in the prefrontal cortex when active processing is required to encode and maintain information in WM representations (Moran et al., 2010; Liebe et al., 2012; Roux and Uhlhaas, 2014; Wallis et al., 2015). Theta activity may be particularly important when multiple stimuli must be temporally ordered or features from different modalities (such as color and spatial location) must be integrated into a single WM representation (Sauseng et al., 2010). Lesions to prefrontal cortex disrupt the generation and propagation of theta activity and results in a degradation in WM performance (Johnson et al., 2017). Causal entrainment of theta activity with noninvasive brain stimulation can boost WM performance, although this has previously been demonstrated with transcranial alternating current stimulation (Jaušovec and Jaušovec, 2014; Alekseichuk et al., 2016; Reinhart, 2017), which lacks the spatial resolution of TMS, or with rhythmic TMS in the context of auditory WM during the delay period (Albouy et al., 2017). Therefore, it remains unclear whether theta activity in the prefrontal cortex plays a causal role in retrospectively prioritizing internally maintained WM representations.

In order to differentiate the encoding of visual information into WM from processes that pertain to the manipulation of maintained representations, we utilized a retro-cue WM paradigm (**Figure 3.1**) (Souza and Oberauer, 2016). In a typical retro-cue WM paradigm, a retro-cue during the delay signals the spatial location of the stimulus that will be tested and should therefore be prioritized within memory. The retro-cue elicits ipsilateral alpha oscillations in parietal cortex and contralateral theta frequency oscillations in prefrontal cortex (Wallis et al., 2015), similar to studies that demonstrate contralateral prefrontal theta activity at encoding (Moran et al., 2010) and ipsilateral parietal alpha activity with contralateral distractors at encoding (Sauseng et al., 2009). Whereas a typical retro-cue study cues a single item, thus requiring suppression of irrelevant information in both hemifields (Wallis et al.), the current study presents separate

stimulus sets in each hemifield and then retro-cues an entire hemifield (**Figure 3.1**). This was designed to completely segregate the prioritized and irrelevant information to separate hemifields and further accentuate the laterality differences in cognitive processing and task-relevant oscillatory activity. Recent evidence suggests that alpha and theta oscillations correspond to distinct cognitive processes and parallel frontoparietal systems, with alpha originating in parietal and theta originating in prefrontal cortex (Johnson et al., 2017), and that these distinct cognitive processes and oscillations are often inversely related (Roux and Uhlhaas, 2014).

Rhythmic TMS has been shown to locally entrain both alpha (Thut et al., 2011) and theta (Albouy et al., 2017) frequency neural oscillations and thus provides a causal method to test the distinct roles of these oscillations in cognitive processing. In the current study, we used a retro-cue WM task designed to drive the lateralized processing of WM representations (suppression or prioritization) and associated task-relevant oscillatory activity (alpha and theta). We applied alpha and theta rhythmic TMS to parietal and prefrontal cortex both ipsilateral and contralateral to the retro-cue. Critically, we predicted that the effect of rhythmic TMS on WM performance would be dependent on whether the applied TMS frequency matched the task-relevant oscillatory activity of the targeted region.

3.3 Results & Discussion

Subjects performed a retro-cue WM task with an initial encoding display with two peripherally presented memory arrays of colored squares in the left and right visual hemifield (**Figure 3.1**; see Methods). After a delay period, a deterministic retro-cue was presented that indicated which memory array would be tested by the probe, or a neutral cue was presented that indicated either array could be tested. Following a second delay period, a single probe array was presented that either matched (half of the trials) or did not match (half of the trials; either a single color was changed or two stimuli swapped positions within the array) the memory array previously presented in that hemifield. Subjects responded match or no match with a button press.

Twenty subjects completed all four sessions of the experiment. An initial behavioral session screened participants for their ability to utilize the retro-cue. The second session collected baseline functional magnetic resonance imaging (fMRI) data while participants performed the retro-cue task. We analyzed the overall task activation in fMRI to localize subject-specific regions of interest (ROIs) in left anterior middle frontal gyrus (MFG) and left inferior intraparietal sulcus (IPS) for TMS targeting in the third and fourth sessions (**Figure 3.1C**). In separate TMS sessions, subjects received TMS to either left MFG or left IPS. Online TMS was delivered in either alpha (10 hertz) or theta (5 hertz) frequency after presentation of the retro-cue (**Figure 3.1D**). To target retro-cue driven processes separate from processes related to the initial encoding of the stimuli into WM representations, TMS was time locked to the time frame for which these oscillatory effects were previously linked to retro-cues (Wallis et al., 2015). To control for non-specific

effects of rhythmic TMS, we also delivered an arrhythmic TMS pattern that matched the duration and number of pulses as rhythmic TMS.

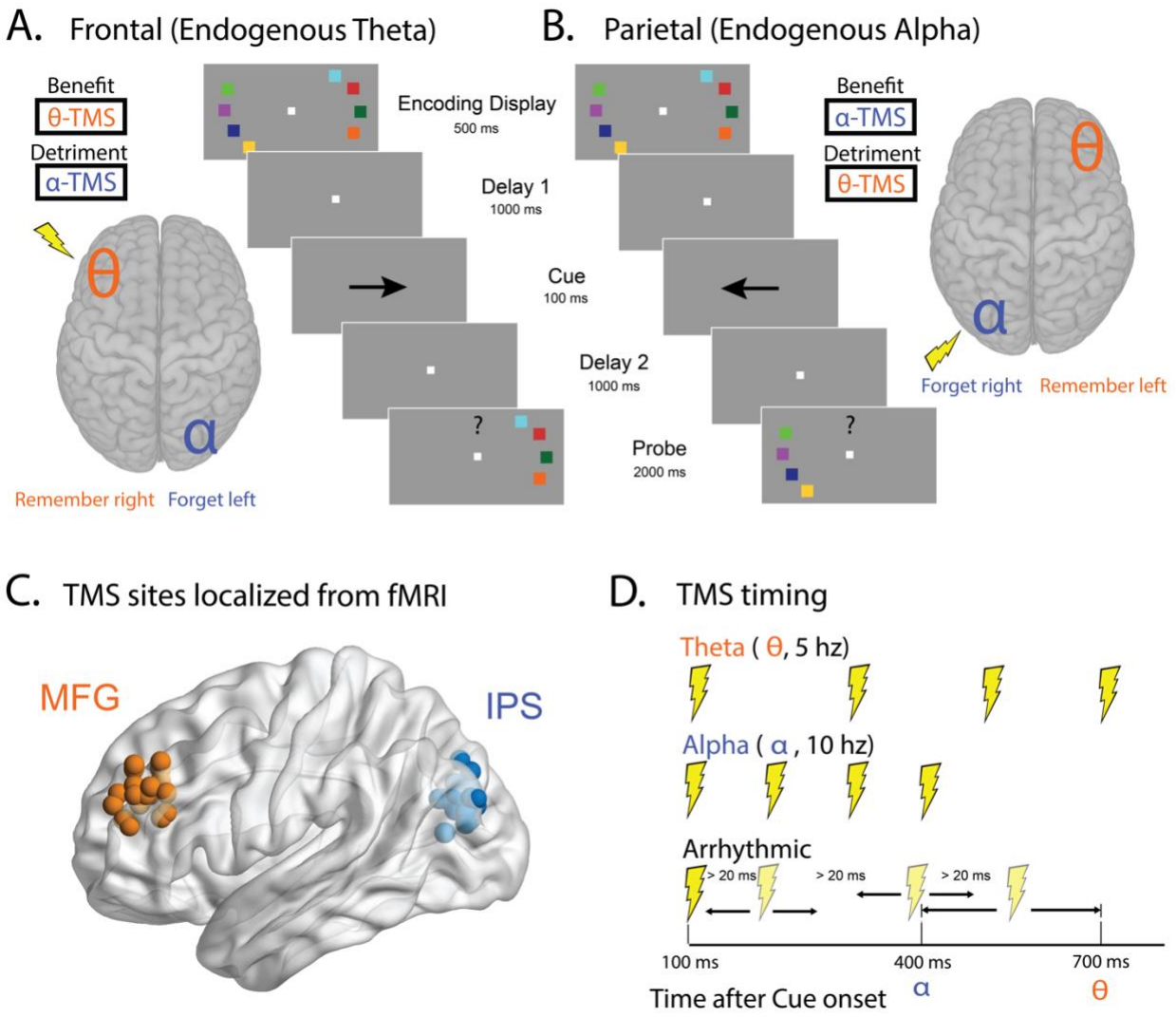

Figure 3.1 Experimental design and hypothesized TMS effects. (**A**,**B**) Model of task-relevant endogenous neural oscillatory activity following a retro-cue to the right (**A**) or left (**B**) visual field in which retro-cues drive theta frequency oscillatory activity in frontal cortex contralateral to the prioritized visual field and alpha frequency oscillatory activity ipsilateral to the prioritized visual field. Rhythmic transcranial magnetic stimulation (TMS) was applied to the left anterior middle frontal gyrus (MFG) and left inferior intraparietal sulcus (IPS) in separate sessions. Critically, this model predicts that the effect of rhythmic TMS on performance will be dependent on whether the TMS frequency matches or mismatches the task-relevant endogenous frequency at that site. (**C**) Prior to the TMS sessions, the left MFG and left IPS sites were localized for each subject using the retro-cue WM task during functional magnetic resonance imaging (fMRI). (**D**) TMS trains were delivered on every trial in either alpha frequency, theta frequency, or an arrhythmic pattern matched for duration and number of pulses. The trains were time-locked to the window after

retro-cue onset during which a previous magnetoencephalography study reported endogenous theta and alpha neural oscillations in MFG and IPS during a similar retro-cue WM paradigm (Wallis et al., 2015).

We assessed the frequency-specific effects of TMS on two behavioral metrics that benefited from the retro-cue during the initial behavioral session: WM capacity and response time (RT). As described above, the retro-cue WM task requires the suppression or prioritization of information in each hemifield and was thus designed to drive lateralized cognitive processing and task-relevant oscillatory activity: theta activity in prefrontal cortex contralateral to the prioritized hemifield (**Figure 3.1A**), and alpha activity in parietal cortex ipsilateral to the prioritized hemifield (**Figure 3.1B**). Therefore, our primary analyses focus on these conditions, specifically: TMS stimulation to prefrontal cortex when the contralateral hemifield is cued, and TMS stimulation to parietal cortex when the ipsilateral hemifield is cued. We predicted that the effect of rhythmic TMS would be dependent on whether the TMS frequency matched the task-relevant oscillatory activity of the targeted region. To test for this interaction, we ran a two-way repeated-measures analysis of variance (ANOVA) with factors of TMS site (prefrontal / parietal) and TMS frequency (alpha / theta) separately for capacity and RT. To control for non-frequency specific effects, each condition was run as the difference from condition-matched arrhythmic TMS. We found a significant interaction for WM capacity ($F(1,19) = 5.66$, $p = 0.028$, $\eta^2_p = 0.23$; **Figure 3.2A**). We did not find a significant interaction for RT ($F(1,19) = 1.32$, $p = 0.27$, $\eta^2_p = 0.065$; **Figure 3.2B**). As a control, we tested for this interaction in the conditions in which we do not predict task-relevant endogenous activity and found no significant effects (see Methods, **Figure 3.2-1**). Together, these findings provide causal evidence to support the hypothesis that the effect of rhythmic TMS critically depends on the task-relevant endogenous activity of the stimulated region. Furthermore, our results provide causal evidence in support of the hypothesis that alpha frequency neural oscillations can actively inhibit WM representations and theta frequency neural oscillations boost WM representations.

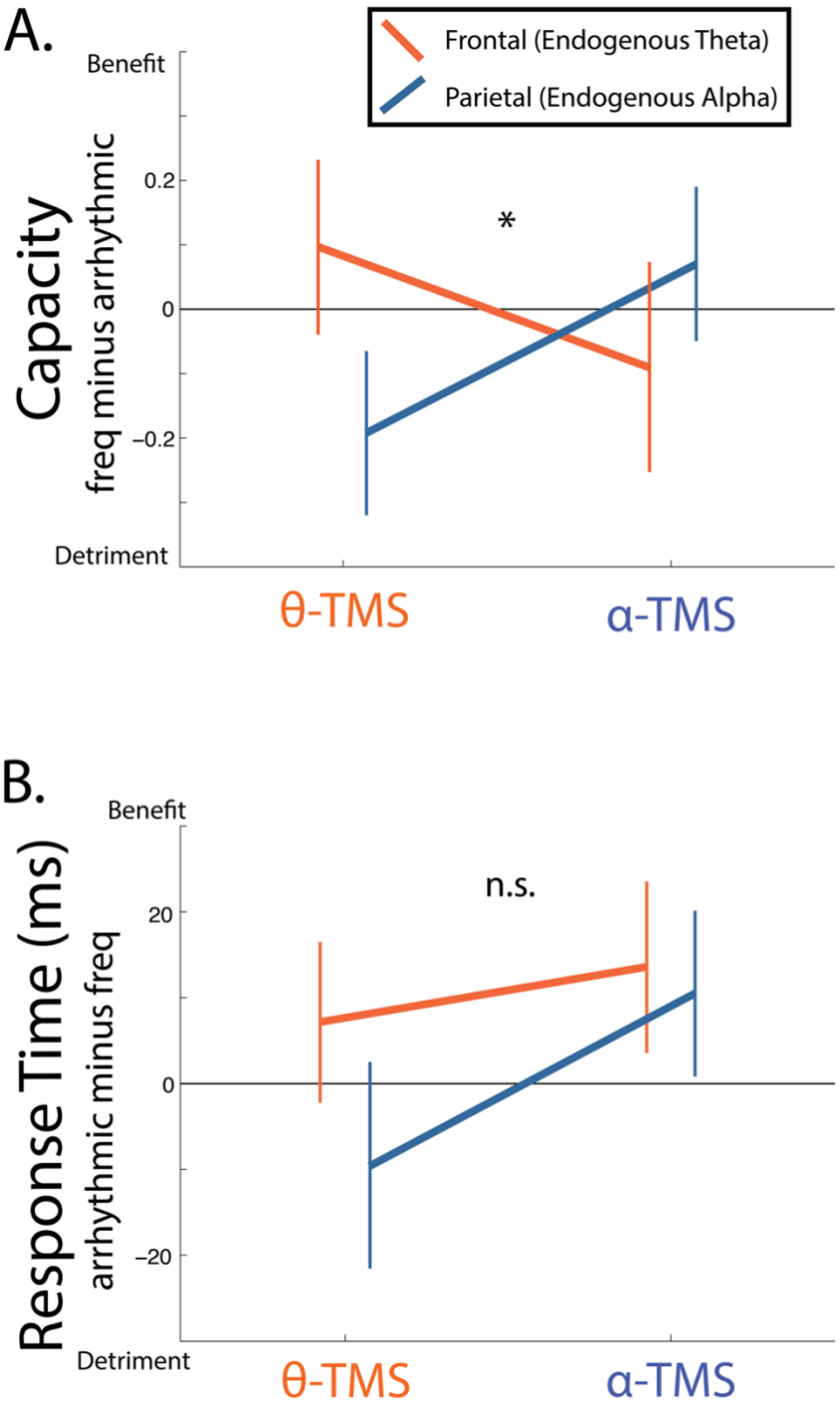

Figure 3.2. Rhythmic TMS effects on WM performance as a function of TMS frequency and targeted region. ANOVA interaction for TMS frequency by TMS site. * $p < 0.05$. Error bars are standard error of the mean. Consistent with the hypothesized effects, we find a significant interaction between region and TMS frequency in WM capacity (**A**). We do not find a significant interaction in response time (**B**).

We hypothesized that fMRI activity within the MFG and IPS ROIs would quantify the degree to which subjects were able to endogenously generate the task-relevant processing and oscillatory activity, and that this should be predictive of the frequency-specific effect during TMS sessions. Critically, we predict brain-behavior correlations of opposite direction across the two regions (positive for frontal cortex and negative for parietal cortex). Specifically, left MFG should exhibit increased brain activity when the contralateral hemifield is prioritized (relative to the neutral cue condition; see Methods). Increased theta frequency neural oscillations correspond to active processing associated with the prioritization of relevant stimuli, and therefore an increase in the blood oxygenation-level (BOLD) signal. Similarly, left IPS should exhibit decreased brain activity in response to a retro-cue that prioritizes the ipsilateral hemifield (relative to the neutral cue condition). Increased alpha frequency neural oscillations correspond to inhibition of brain activity associated with the suppression of irrelevant stimuli, and therefore a decrease in the BOLD signal. In left MFG, brain activity parameter estimates significantly correlated with the theta TMS effect ($r(18) = 0.55$, $p = 0.014$, **Figure 3.3A**). For left IPS, brain activity parameter estimates did not significantly correlate with the alpha TMS effect ($r(18) = -0.35$, $p = 0.139$, **Figure 3.2B**). However, the interaction of these correlations was significant ($z(18) = 3.61$, $p = 0.0003$). As a control analysis, we found that this effect is not present for trials in which endogenous activity is not systematically driven by cognitive demands (see Methods; **Figure 3.3-1**). These findings further emphasize the importance of endogenous activity on frequency-specific TMS effects: fMRI activity for the task-relevant conditions (measured prior to TMS sessions) predicted the ultimate behavioral effect of rhythmic TMS, suggesting that subjects with stronger task-relevant endogenous activity were more susceptible to frequency-specific TMS that matched or mismatched the internally driven state. Electrophysiology has long exhibited prominent theta frequency oscillations emanating from the prefrontal midline and alpha frequency oscillations emanating from the parietal-occipital midline (Klimesch et al., 1996). Despite the prominence of these oscillation at the midline, previous work has demonstrated that rhythmic TMS to the electrode with peak EEG power in the targeted frequency band did not produce behavioral effects, whereas rhythmic TMS to a region localized by fMRI did impact behavior (Sauseng et al., 2009). This is consistent with our brain-behavior correlations and provide support for choosing TMS target sites motivated by fMRI results, as we have done in the present study.

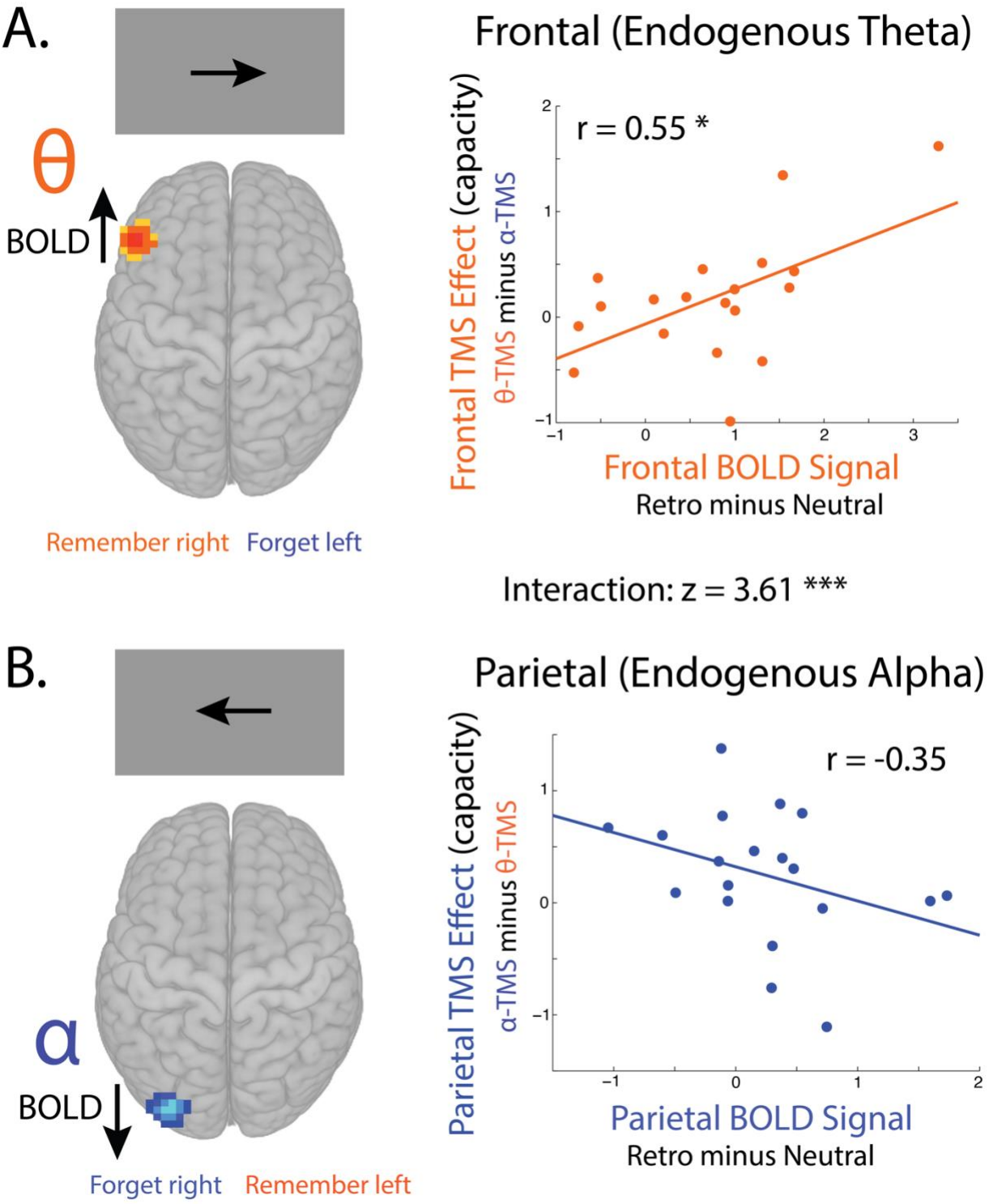

Figure 3.3. Functional MRI blood oxygenation-dependent (BOLD) signal in frontal and parietal cortex predicted frequency-specific effect of TMS only when task-relevant endogenous activity was systematically manipulated. Critically, we predicted brain-behavior correlations of opposite direction across the two regions (positive for frontal cortex and negative for parietal cortex).

Specifically, left frontal cortex should exhibit increased brain activity when the contralateral hemifield is prioritized (relative to the neutral cue condition; see Methods). Increased theta frequency neural oscillations correspond to active processing associated with the prioritization of relevant stimuli, and therefore an increase in the BOLD signal. Similarly, left parietal cortex should exhibit decreased brain activity in response to a retro-cue that prioritizes the ipsilateral hemifield (relative to the neutral cue condition). Increased alpha frequency neural oscillations correspond to inhibition of brain activity associated with the suppression of irrelevant stimuli, and therefore a decrease in the BOLD signal. We found a significant correlation for frontal theta, but not for parietal alpha. However, the interaction between these correlations was significant. * $p < 0.05$, *** $p < 0.0005$.

Our frequency specific TMS effects provide causal evidence consistent with prior observations that alpha and theta neural oscillations are often anti-correlated within a region of cortex (Roux and Uhlhaas, 2014). Recent evidence on alpha and theta frequency network dynamics suggests that different networks entrain to alpha for distractor suppression and to theta for active processing during WM at high load (Dai et al., 2017). A prominent theory proposes that alpha frequency oscillations reflect thalamo-cortical feedback loops for inhibiting active processing while theta frequency oscillations reflect hippocampal-cortical feedback loops that engage long term potentiation processes important for encoding new information (Klimesch, 1999). Under this interpretation, alpha and theta network oscillatory signatures are fundamentally incompatible. The presence of an inhibitory signal in alpha or an excitatory signal in theta frequency precludes the other from occurring as the underlying neural architecture cannot support both. By entraining alpha frequency oscillations in a region that required active theta frequency processing given task demands, we impaired the activity of that region. In complement, by stimulating in theta frequency to a region that required alpha frequency suppression of activity based on task demands, we released that region from inhibitory suppression leading to a detriment in performance.

The neural basis of retro-cues and prioritization within WM is an area of substantial active debate. Recently, Myers et al. 2017 put forth a model proposing four stages involved with the prioritization process (Myers et al., 2017). The first stage involves encoding information into WM representations at the primary site of processing for that information type, e.g. visual cortex for visual information. Next the frontal-parietal network acts to transiently orient selective attention to the relevant items held in WM and inhibits irrelevant regions of cortex. Third, the frontal parietal network in tandem with the cingulo-opercular network reformats the WM representation into a more abstract and accessible representations that is then held in focus in prefrontal cortex (Myers et al., 2017). Finally, the locus of the WM representation is shifted to the prefrontal cortex and signaling from lateral prefrontal cortex is sufficient to reactivate the relevant WM representations. Although we did not directly test this model in our experiment, we find causal evidence that alpha frequency neural oscillations could be the mechanism by which selective attention inhibits low priority representations (in the second stage) while disinhibiting high priority representations via desynchronization. Furthermore, we found causal evidence to support the theory that theta frequency oscillations in prefrontal cortex prioritize WM representations and improve capacity, which is compatible with the proposal that prefrontal

cortex contains an abstract code (in the third and fourth stages). We speculate that theta frequency stimulation to lateral prefrontal cortex may enhance the process by which frontal-parietal cortex reformats the high-fidelity WM representations maintained in sensory regions (Lisman and Jensen, 2013; D'Esposito and Postle, 2015; Myers et al., 2017).

Working memory deficits are symptomatic in a variety of mood disorders (Rose and Ebmeier, 2006). Noninvasive brain stimulation offers an alternative method of intervention for patients that are non-responsive to pharmaceuticals (Perera et al., 2016). In the current experiment, we demonstrate a region by TMS frequency interaction such that the benefit or detriment to cognition is crucially dependent on the frequency and site of stimulation. If attempting to boost working memory, for example, then the incorrect frequency of stimulation could reverse the direction of the effect and benefits may be maximal when the frequency matches the endogenous activity. The field of clinical noninvasive brain stimulation could benefit enormously by adjusting stimulation parameters to more accurately target the pathological system in question.

3.4 Materials and Methods

3.4.1 Participants

We obtained informed consent from thirty-seven research participants according to the guidelines of the Committee for the Protection of Human Subjects and University of California, Berkeley. Eight of the 37 subjects were excluded from the fMRI and TMS sessions because they did not show a beneficial effect of the retro-cues in a behavioral screening session. An additional nine subjects dropped out of the study due to an inability to make the time commitment required to complete all sessions. Twenty subjects (7 males, ages mean 21.3 years and standard deviation 3.1 years) completed all four sessions of the experiment and were included in the final analyses.

3.4.2 General Procedure and Behavioral Task

The overall experimental design included four sessions: an initial behavior-only session to screen participants for their ability to perform the task, a functional magnetic resonance imaging (fMRI) scan to localize regions of interest to be targeted by subsequent TMS sessions, and two TMS sessions with online stimulation of left MFG and IPS, counterbalanced for order across participants. Each session was completed on a separate day.

In the initial behavioral screening, participants completed a change detection WM task with retro-cues (**Figure 3.1A**). On each trial, two arrays of colored squares were presented around a central fixation cross for 500 ms. The two memory arrays were always on opposite sides of the visual field and each item was equidistant from fixation. The left and right arrays included an equal number of stimuli (two, three, or four items per array) on each trial. Following a delay period of 1000 ms, a retro-cue (50% of trials) or a neutral cue (50% of trials) was presented at fixation for 100 ms. Retro-cues took the form of an arrow pointing towards either the left or right

visual field. Participants were instructed to "remember" the array from the cued visual field and to "forget" the array from the other visual field; the retrospective cue was 100% predictive of the array that would be tested at probe. Neutral cues took the form of a double-sided arrow that provided no predictive information about the upcoming memory probe; participants were instructed to continue remembering both arrays. After a second delay period of 1000 ms, subjects were probed with a test array on either the left or right side of fixation, in the exact same location as the original encoding display. Participants indicated whether the entire test array matched the memory array or whether at least one color had changed. On non-match trials the test array could include a novel color not in either memory array, a color from the memory array not tested, or two colors in the array could have swapped. Subjects had 2000 ms to indicate their response by making a button press with the index finger (match) or the middle finger (non-match) of their right hand. The conditions for size of memory array and retro versus neutral cue were intermixed, randomized, and balanced.

We used a fixed stimulus set of nine colors. The colored squares could appear at 12 different locations equally space around fixation. On each trial, the two memory arrays were randomly placed contiguously in each visual hemifield, six possible locations each. The memory arrays were never contiguous to each other within the encoding display and therefore always had at least one empty location between them. For the screening session, participants had on average 90.32 +/- 30.36 trials per condition with a minimum of 36 trials per condition.

As an initial assessment of performance, we compared performance between retro and neutral cues for response time and accuracy. At the group level, participants demonstrated a behavioral improvement from the retro-cue relative to the neutral cue: increased accuracy ($t(36) = 6.10$, $p = 5.85 \times 10^{-7}$, $d = -1.92$) and decreased response time ($t(36) = -11.70$, $p = 7.95 \times 10^{-14}$, $d = 1.00$). Next, individual subjects were screened for their ability to utilize the retro-cue by comparing their performance to the non-informative neutral cue. We performed this screening process so that participants included in the TMS sessions would be more likely to show a retro-cue benefit and be generating the endogenous neural oscillatory signatures targeted by rhythmic TMS. Out of the 37 subjects screened, eight displayed suboptimal behavioral such that retro-cue performance was worse than or equal to that of the neutral cue and thus did not participate in the fMRI and TMS sessions of the study.

For the TMS sessions, the behavioral task was restricted to a single set size that that was determined on a participant-specific basis based on their performance in the initial session. This procedure was designed to maximize the effect of TMS on behavior by avoiding floor and ceiling effects on performance. Participants who did not show a retro-cue benefit for a set size of four, but demonstrated a retro-cue benefit for a set size of three were given encoding displays matched to their optimal performance at size three for all subsequent sessions. All other participants were assigned to a set size of four. Of the 20 subjects that completed all session and were included in analyses, eight were assigned to a set size of three.

3.4.3 fMRI and Region of Interest Localization Procedure

After the behavioral screening session, subjects underwent an MRI session in order to acquire a high resolution anatomical scan for 3D stereotaxic navigation and to functionally localize the left middle frontal gyrus (MFG) and left inferior intraparietal sulcus (IPS) for targeting during subsequent TMS sessions. Participants performed the same task as the behavioral screening session except with a fixed set size based on their screening session, and completed three to six runs depending on time constraints of the fMRI procedure. Each run consisted of 40 trials. Overall, each subject had at least 30 trials, mean 47.89, in each of 4 conditions: probe on the left or right visual field and cue type (retro or neutral).

MRI data was collected in the Henry H. Wheeler Brain Imaging Center at the University of California, Berkeley on a Siemens 3T MAGNETOM Trio (Erlangen, Germany) using a 32-channel receive-only coil. We collected a high resolution structural scan for targeting of TMS and multiple functional MRI scans for localizing the subject-specific task-activated left MFG and IPS. The anatomical scan was collected using a T1-weighted magnetization-prepared rapid gradient-echo (MPRAGE) sequence with 160 sagittal slices with 1 mm isotropic voxels, 2.3 second repetition time, interleaved slice acquisition, phase-encoding direction from anterior to posterior, 2.98 millisecond echo time, 9-degree flip angle, and parallel imaging via GeneRalized Autocalibrating Partial Parallel Acquisition (GRAPPA) with an acceleration factor of 2. The functional echo planar imaging scans were collected during performance of the WM task using a T2*-weighted single-shot echo-planar imaging (EPI) sequence with 2.5 mm isotropic voxels, 2.5 second repetition time, descending slice acquisition, phase encoding direction anterior to posterior, 29 millisecond echo time, 60-degree flip angle, fat saturation, and prescan normalization. The first two volumes of every functional run were discarded upon acquisition; and for analysis purposes, the first two recorded volumes were also discarded.

Preprocessing of fMRI data was performed using the Statistical Parametric Mapping 12 toolbox (SPM12, www.fil.ion.ucl.ac.uk/spm) in MATLAB (version 2014a release). All preprocessing steps were performed in SPM12 unless otherwise noted. The anatomical image had the neck removed (AFNI, afni.nimh.nih.gov), manual reorientation to the anterior commissure, segmentation with mean bias correction, and normalization into the Montreal Neurological Institute (MNI) space. The functional data were de-spiked at three standard deviations above the mean (AFNI, afni.nimh.nih.gov), slice time corrected, rigid body motion aligned to the mean functional image, manually reoriented to the anterior commissure, normalized into MNI space, and smoothed with a FWHM kernel of 4 millimeters.

A univariate analysis of the fMRI data was performed in MNI space with a general linear model (GLM) analysis that included a regressor for each behavioral condition (retro-cue probe left, neutral-cue probe left, retro-cue probe right, and neutral-cue probe right) and a regressor for missed trials. Each trial was modeled as a boxcar with onset at the presentation of the encoding display and duration until the subject made a response (mean response time relative to the onset of the test probe was 967.3 ms with a standard deviation of 125.9 ms). If no response was made, then the boxcar duration included the full two second response window. The above regressors were convolved with the canonical hemodynamic response function. We also included 8 nuisance

regressors: 6 rigid body motion realignment parameters and the mean signal in white matter and cerebral spinal fluid. The masks for white matter and cerebral spinal fluid were calculated by SPM12's segmentation of the anatomical image.

Coordinates used for TMS targeting were defined individually for each subject based on a combination of task activity and coordinates reported by a meta-analysis of retro-cue studies that identified clusters in MFG (-40, 39, 23) and IPS (-34, -76, 26) (Wallis et al., 2015). Each TMS targeting coordinate was defined as the peak univariate BOLD activation in the contrast map for a contrast comparing all four task conditions versus baseline that was nearest to the meta-analysis coordinates and constrained anatomically to the middle frontal gyrus and inferior intraparietal sulcus. A starting threshold of $p < 0.001$ was initially selected and then lowered until a supra-threshold cluster was found for each subject. The mean coordinates across subjects for left MFG in MNI space was (-33.70, 42.70, 27.70) with a standard deviation of (6.10, 6.03, 6.63) and for left IPS was (-30.60, -78.80, 23.80) with a standard deviation of (3.90, 4.18, 6.19) (**Figure 3.1C**). After the subject-specific coordinates were defined in MNI space, we created an eight-millimeter sphere surrounding this point and these regions of interest were back-normalized into native space for online TMS targeting.

3.4.4 Non-invasive Brain Stimulation

For the third and fourth sessions of the experiment, online rhythmic TMS was delivered to either left MFG or IPS on separate days, counterbalanced for order, using a MagStim Super Rapid-2 Plus1 stimulator with a MagStim figure-eight 70mm double air film coil (MagStim, Whitland, United Kingdom). Each participant's motor threshold (MT) was calculated to calibrate the coil intensity to their specific sensitivity level. To calculate MT, an electrode was attached to the first dorsal interosseous muscle on the right hand of the subject. Single pulses of TMS were delivered to the corresponding hand region of the left motor cortex at a 45 degree angle until the TMS pulses reliably elicited a motor evoked potential (MEP), defined as a near instantaneous voltage increase of at least 70 microvolts above baseline (O'Shea et al., 2007). Once an MEP was generated, the intensity was decreased to a level that elicited an MEP on 5 out of 10 TMS pulses.

A custom-built cable triggered trains of 4 biphasic pulses at 110% of MT in either 5 hertz (theta frequency), 10 hertz (alpha frequency), or arrhythmic. During online TMS, participants were actively monitored for signs of duress and were encouraged to inform the experimenter of any discomfort. To ensure the accuracy of TMS targeting, we used Rogue Research's BrainSight v2.2.11 (Rogue Research, Montreal, Canada) with a Northern Digital Polaris Spectra infrared camera (Waterloo, Ontario, Canada) to register anatomical landmarks on the participant's head to their anatomical MRI scan with stereotaxic 3-dimensional tracking. Subject-specific coordinates derived from that individual subject's fMRI data were overlaid on the subject's anatomical image. A trajectory for TMS was calculated perpendicular to the skull. The coil angle was held constant in the posterior to anterior direction for both TMS sites. During the TMS sessions, experimenters actively maintained a stable position of the TMS coil aided by a MagStim coil holder and continuous real-time stereotaxic tracking. After the delivery of each TMS train, a

TTL pulse was generated that recorded the position of the coil relative to the target trajectory. Trials were rejected from analysis in which the TMS coil position deviated greater than 5 millimeters from the target trajectory (mean 1.66% with standard deviation 2.19% of trials were removed).

Wallis et al 2015 found behaviorally relevant alpha frequency oscillations from 300 to 800 milliseconds and theta frequency oscillations from 100 to 600 milliseconds after the onset of the retro-cue (Wallis et al., 2015). Based on the timing of these oscillations, we delivered a train of TMS 100 milliseconds after the onset of the retro-cue to maximally overlap with both of these relevant time windows (**Figure 3.1D**). Each biphasic TMS pulse was a brief event lasting only about one fourth of a millisecond. Thus, an alpha frequency train consisted of four pulses of TMS with an inter-pulse interval of 100 milliseconds (10 hertz) and total duration of 300 ms, and theta frequency TMS consisted of four pulses of TMS with an inter-pulse interval of 200 milliseconds (5 hertz). Arrhythmic TMS was used as a control stimulation to match any non-frequency specific physiological effects of receiving TMS pulses in the same window of time. The total duration of arrhythmic TMS varied uniformly between that of alpha and theta frequency TMS (300 to 600 milliseconds). Arrhythmic TMS trains were constrained such that each pulse was separated by at least 20 milliseconds. Each arrhythmic train was generated randomly and checked for its proximity to either alpha or theta frequency pulse patterns. A generated pulse pattern was discarded if all three intervals had values in the range of 80-120ms or if all three intervals had values in the range of 180-220 ms, and a new pattern was randomly generated. In order to control for non-frequency-specific effects of online TMS within each participant, we computed differences scores for each condition by contrasting alpha/theta TMS versus arrhythmic TMS, e.g. retro-cue right-side trials that received alpha TMS to MFG minus retro-cue right-side trials that received arrhythmic TMS to MFG. These differences scores were used for all statistical analyses. This procedure also controls for differences in set size across subjects.

To maximize statistical power, the TMS sessions had a fixed set size and only retro-cues. Each task block during the TMS sessions contained 48 trials of six conditions (theta TMS probe-right, alpha TMS probe-right, arrhythmic TMS probe-right, theta TMS probe-left, alpha TMS probe-left, and arrhythmic TMS probe-left). For each TMS session, subjects completed eight blocks of 48 trials. Overall, each participant completed 384 trials in each TMS session for a total of 64 sessions in every experimental condition.

3.4.5 Primary data analysis

To control for differences in set size and given that we used the full memory array for our probe, we calculated performance using Pashler's metric for capacity (Rouder et al., 2011). Pashler's capacity is calculated as the memory load multiplied by the hit rate (correct responses during match trials) multiplied by the false alarm rate (correct rejection during a non-match trial) divided by one minus the false alarm rate.

Our primary analysis was to test for frequency specific effects of TMS for conditions in which we expected task-relevant endogenous activity driven by our cognitive manipulation. For TMS to MFG, we used conditions with a right-side (contralateral) retro-cue. For TMS to IPS, we used conditions with a left-side (ipsilateral) retro-cue. We performed a two by two (TMS site by TMS frequency) repeated-measures analysis of variance (ANOVA) for capacity and response time.

As a control analysis, we tested for frequency specific effects of TMS for conditions in which the endogenous activity was unknown and not driven by our cognitive manipulations. For TMS to MFG, we used conditions with a left-side retro-cue (**Figure 3.1-1A**). For TMS to IPS, we used conditions with a right-side retro-cue (**Figure 3.1-1B**). We performed a two by two (TMS site by TMS frequency) repeated-measures ANOVA for capacity and response time. As expected, there was no interaction for either capacity ($F(1,19) = 1.91$, $p = 0.18$, $\eta^2_p = 0.091$; **Figure 3.2-1A**) or response time ($F(1,19) = 1.09$, $p = 0.31$, $\eta^2_p = 0.054$; Figure 2-1B). These findings further emphasize the importance of driving endogenous activity when applying noninvasive brain stimulation.

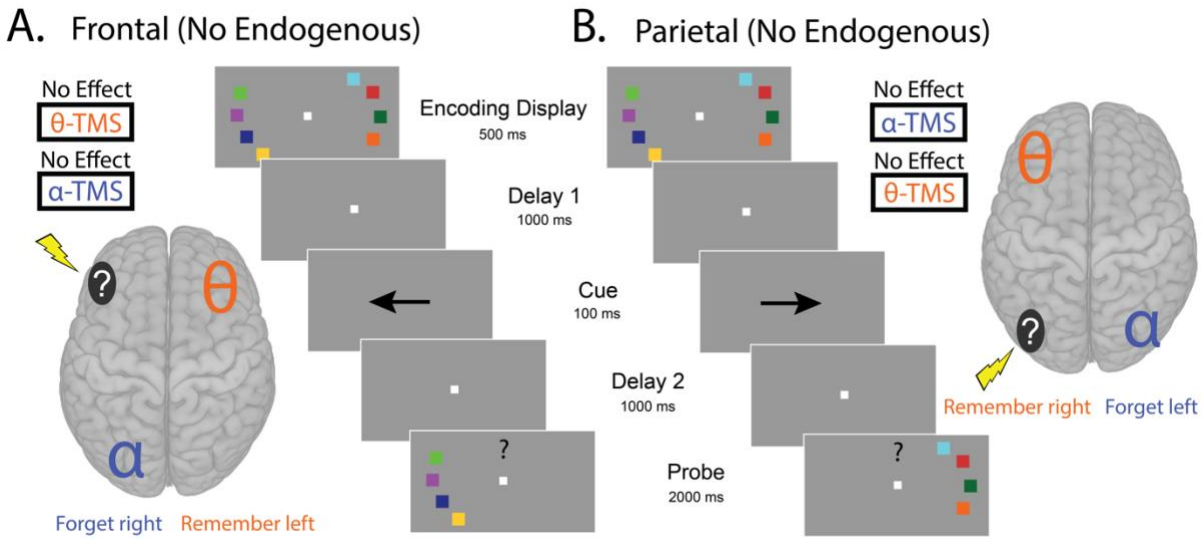

Figure 1-1. When task-relevant endogenous activity in a region is not driven by our cognitive manipulation, we do not expect to find a systematic effect of rhythmic TMS.

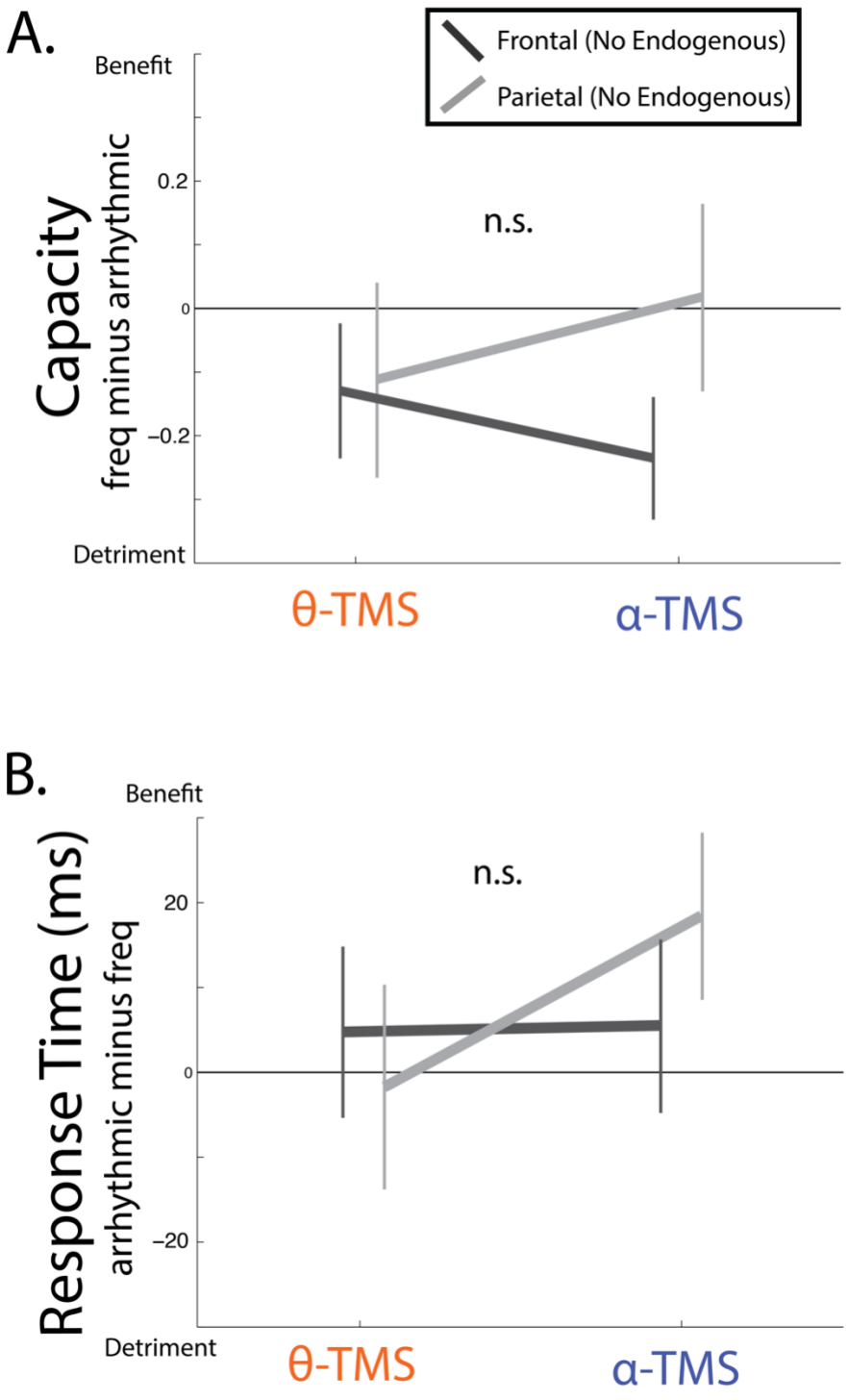

Figure 3.2-1. When task-relevant endogenous activity in a region is not driven by our cognitive manipulation, we did not find an interaction of TMS site by TMS frequency for capacity (**A**) or response time (**B**).

3.4.6 Brain-behavior correlation analyses

To assess ROI activity for each condition, we first defined MFG and IPS ROIs for each participant by creating a sphere of radius eight mm centered around the participant's TMS target coordinates. We then took the mean of the parameter estimates (beta value) across the ROI for each condition in the GLM. These mean values were then used to create two contrasts for correlation analyses. For the MFG ROI, we contrasted the retro-cue right-side condition minus the neutral-cue right-side condition. For the IPS ROI, we contrasted the retro-cue left-side condition minus the neutral-cue left-side condition. Each of these contrasts differs on the feature of interest (retro-cue) but controls for visual stimulation and the hemifield of the test probe. One participant had activity more than three standard deviations below the mean for the MFG ROI contrast and was thus omitted from both brain-behavior correlations. These measures of brain activity were then correlated with specific TMS effects: activity in the MFG ROI was correlated with the behavioral effects of theta frequency TMS to MFG for retro-cues to the right visual field minus alpha frequency TMS to MFG for retro-cues to the right visual field. Activity in the IPS ROI was correlated with alpha frequency TMS to IPS for retro-cues to the left visual field minus theta frequency TMS to IPS for retro-cues to the left visual field. One subject was removed from this analysis because their difference in MFG activation for retro versus neutral cue was greater than three standard deviations from the mean.

As a control for the brain behavior analysis, we correlated brain activity in the MFG ROI for retro-cues with a probe in the left visual field minus neutral-cues with a probe in the left visual field to the behavioral effects of theta frequency TMS to MFG with retro-cues to the left visual field minus alpha frequency TMS to MFG with retro-cues to the left visual field ($r(18) = 0.06$, $p = 0.794$; **Figure 3.3-1A**). For IPS, we correlated brain in the IPS ROI for retro-cues with a probe in the right visual field minus neutral-cues with a probe in right visual field to the behavioral effects of alpha frequency TMS to IPS with retro-cues to the right visual field minus alpha frequency TMS to IPS with retro-cues to the right visual field ($r(18) = -0.26$, $p = 0.263$; **Figure 3.3-1B**). The interaction between these control correlations was also not significant ($z(18) = 1.05$, $p = 0.29$).

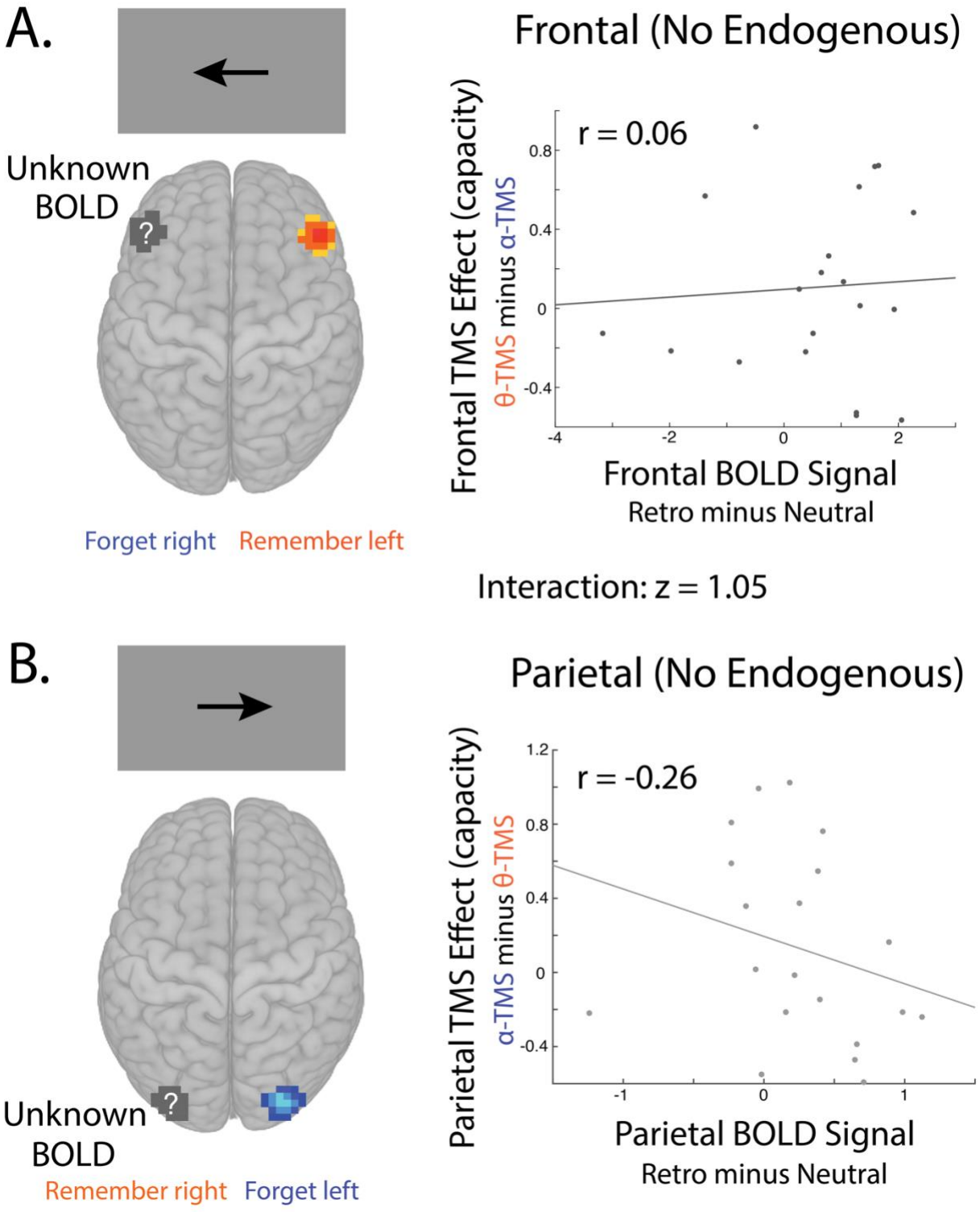

Figure 3-1. When task-relevant endogenous activity in a region is not systematically driven by our cognitive manipulation, there was neither a predicted BOLD signal effect, nor rhythmic TMS effect. As expected, we found no correlation between BOLD signal and TMS effect, and no interaction between the TMS sites and rhythmic TMS frequencies.

%% SECTION 2 %%

SIMULTANEOUS TMS-fMRI

Chapter 4

DEVELOPING A METHODOLOGY FOR CONCURRENT TMS-FMRI: CAUSAL EVIDENCE FOR FRONTAL-STRIATAL LOOPS

4.1 Abstract

Transcranial Magnetic Stimulation (TMS) allows for direct activation of neurons in the human neocortex and has proven to be fundamental for causal hypothesis testing in cognitive neuroscience. It has yet to be shown that spreading activation from TMS is confined to anatomically specific circuits and whether cortical TMS can reliably activate connected subcortical structures. By administering TMS simultaneously with functional Magnetic Resonance Imaging (fMRI), the effect of cortical TMS on activity in subcortical structures can be quantified by varying the levels of TMS output intensity. Concurrent TMS generates significant noise within the fMRI environment and their complex interaction warrants caution before interpreting findings. We present the methodological challenges involved with concurrent TMS-fMRI and provide a solution that minimize induced artifacts. We further suggest measures to quantify and correct for systematic noise. As a proof of this method and to establish the spread of TMS effects, the basal ganglia are targeted because of their distinct anatomically defined circuits with neocortex, or "loops". For sensorimotor processing, primary motor cortex (M1) forms a loop with the putamen, while lateral prefrontal cortex (PFC) forms a loop with the caudate. Strafella et al. (2001, 2003) demonstrated that following TMS to M1 or DLPFC, there is increased dopamine release in posterior putamen or dorsal caudate respectively, as measured by positron emission tomography. In our experiment, two separate groups of healthy human subjects participated in concurrent TMS and resting state fMRI while receiving TMS to either PFC or M1. We found that increasing TMS intensity to the DLPFC resulted in increased MR signal in the dorsal caudate with no change in the posterior putamen. In contrast, TMS to M1 increased BOLD signal in the posterior putamen with no change in the dorsal caudate. These results demonstrate that our methodology effectively addresses the noise induced by simultaneous TMS-fMRI and demonstrates the efficacy of TMS to target deep brain structures with known anatomical connectivity with cortical regions.

4.2 Introduction

Transcranial magnetic stimulation (TMS) allows for causal manipulation of the brain by induced electrical current in a focal region of the brain (Wagner et al., 2009b). Due to its high spatial (<1 centimeter) and temporal resolution (<1 millisecond), this methodology has proved essential for testing the purported cognitive role of a region of the brain (Walsh and Cowey, 2000). However, the question of whether the effect of TMS are local to the targeted region or if they spread throughout a functional or structural brain network is still not fully understood (Romei et al., 2016b). Within a highly interconnected and dynamic brain, perturbation of activity within a single

brain region could have far reaching neural effects and there is limited evidence to this effect. By combining TMS with simultaneous functional magnetic resonance imaging (fMRI), the specific effect of TMS on local and distant brain activity can be empirically tested.

Since the first studies at the end of the 20th century (Bohning, 1999; Bohning et al., 2003), the extent of signal corruption to MRI images that rely on homogenous magnetic fields from applying a strong magnetic field with TMS has been appreciated. Efforts have been made to address the complex interaction interaction of TMS and fMRI (Bungert, 2010; Bestmann et al., 2012). Altogether there are less than 100 experimental studies to date that utilize simultaneous TMS-fMRI, despite almost 20 years since its advent. The slow growth of this promising methodology is most likely due to an absent consensus of which setup is the most effective and a rigorously tested methodology has yet to emerge. Furthermore, labs hoping to purchase the required equipment and start collecting data are met with the sometimes unexpected challenge of re-inventing their own setup with many non-trivial design decisions. In this paper, we provide a thorough discussion of the artifacts that arise from concurrent TMS-fMRI (https://github.com/Brain-Imaging-Center/TMS-fMRI), a method for parameter selection, and a method for minimizing and removing scanner artifacts that arise (with codebase: https://github.com/JustinRiddle). We also provide suggestions for future research to ensure that TMS effects on blood oxygenation-level dependent (BOLD) signal are not false positives induced by signal dropout timed to the event of interest. We suggest quality assurance protocols to monitor for the emergence of artifacts with prolonged use of the MR-compatible TMS coil. Using this methodology, we provide a proof of concept experiment which demonstrates the effectiveness of this method for inducing local activity and the activation of single synapse connections within anatomically known circuits.

Previous evidence from positron emission tomography (PET) demonstrated that TMS to the motor cortex and prefrontal cortex resulted in the extracellular release of dopamine in the posterior putamen and dorsal, anterior caudate respectively (Strafella et al., 2001; 2003). These findings are consistent with structural connectivity studies that find an anterior to posterior gradient mirrored in the frontal cortex and striatum such that PFC projects to anterior caudate and M1 projects to posterior putamen (Draganski et al., 2008; Jarbo and Verstynen, 2015). After developing a method for continuous fMRI acquisition with concurrent trains of 10 hertz repetitive TMS, we targeted the primary motor cortex functionally connected to the left hand and the anterior middle frontal gyrus of the prefrontal cortex. We hypothesized that TMS during open-eyed resting state would activate the region targeted by TMS and that the single synapse anatomical projections in the basal ganglia would also be activated.

4.3 Technical Considerations

TMS delivered during MRI sequence acquisition can lead to a variety of artifacts that are summarized in **Table 4.1**. As we shall explain, some of these artifact sources can be mitigated through timing. Some, however, require reengineering of the TMS coil or its power source. We describe here the principal artifact sources we encountered, and describe how we avoided or dealt with them.

Origin	Artifact description	Temporal characteristics
TMS coil	Vibration	Milliseconds
TMS coil	Thermal drift	Minutes
TMS coil	RF shading	Persistent
TMS coil	Magnetic susceptibility	Persistent
TMS power source	Leakage current	Milliseconds
TMS power source	Asymmetric biphasic pulse*	< 1 ms
TMS to MR hardware coupling	Receive coil to TMS coil coupling	Microsec - millisec
TMS to MR hardware coupling	Eddy currents in MRI hardware	Microsec - seconds
TMS to MR hardware coupling	Transmitter coil to TMS coil coupling	
TMS to subject coupling	Perturbation of M_0 via an effective precessional field	Millisec - seconds
TMS to subject coupling	Flow/diffusion weighting*	< 1 sec
TMS to subject coupling	Perturbation of T_1 steady state	Seconds
Statistical artifacts	TMS coil artifacts	2-4 seconds
Statistical artifacts	Slice artifacts	Single volume

Table 4.1. Categorization and description of principal artifacts arising in a simultaneous TMS-fMRI experiment. Methodological artifacts may arise by virtue of interactions between the intense magnetic fields of each separate method. Artifacts originating in the TMS coil or power supply may be reduced or eliminated in the future through improved hardware designs. Artifact sources indicated with an asterisk apply only when TMS pulses are applied during the EPI readout.

A major issue with in situ TMS is a leakage current during the inter-pulse delay. Commercial TMS power supplies use large capacitors to produce the high current and rapid pulse rates required for TMS protocols. The capacitor must recharge after each TMS pulse while the switching

thyristor is in its open state. Unfortunately, thyristors are not perfect switches and significant current can leak through the switch while in the open state and consequently through to the TMS coil as the capacitor charges, causing the TMS coil to produce a magnetic field. For our TMS machine (see Methods), a MagVenture system upgrade was installed which reduces the leakage current by using a relay-diode combination inserted in the TMS circuit that shorts the leakage current, reducing the leakage current by an order of magnitude. While the intensity of leakage current magnetic fields is several orders of magnitude smaller than the TMS pulses and is of minor consequence from the perspective of brain stimulation, the spurious leakage current magnetic field is sufficiently large to perturb magnetization during EPI. Given the subtle changes in the BOLD signal often measured by fMRI experiments, these leakage currents can produce significant local image disturbances near the TMS coil, particularly in the 10 to 20 milliseconds after a TMS pulse as the capacitor recharges. We take this delay into account in the specific timing used in our experiments.

A methodological concern for TMS-fMRI is the potential for eddy currents in MRI hardware, especially in the steel cryostat containing the main magnet. The TMS coil is designed such that high voltage current passing through its figure-8 coils generates a powerful magnetic field (around 1.5 Tesla near the surface of the coil). This magnetic field induces an electric field that couples to neurons and perturbs their behavior. However, the induced electric field also interacts with the TMS coil itself and conductive elements of the MRI hardware in the same manner. Eddy currents are localized magnetically-induced electric currents in the TMS coil, MR receive coil, and the MRI magnet cryostat. The magnitude of any eddy currents will depend on the distance of the TMS coil to the conductive component, while the time constants of any eddy currents thus produced will depend on the geometry and electrical conductivity of the structure. So far, we have not observed pronounced eddy current effects in our experiments - leakage currents dominate - but it is important to keep this artifact source in mind for certain experimental setups.

Vibration of the TMS coil is a further concern for simultaneous TMS-fMRI. The slight change in the acoustic report of a TMS pulse applied inside an MRI scanner compared to its sound outside the scanner, in the earth's magnetic field, is a related phenomenon. The TMS coil comprises a large figure-8 copper coil. The vibrations arise from the coupling of current within the TMS coil to the main static field of the MRI scanner. As the TMS pulse is applied the current through the TMS coil windings experiences a Lorentz force. This force can set into motion any of the possible vibrational and ballistic modes of the coil's mechanical structure. The TMS coil figure-8 geometry is designed to achieve zero net force on its center of mass as well as zero net torque about its center of mass. In addition, the windings of the coil are potted in a rigid medium to reduce vibrations of the coil windings. The degree to which the TMS pulse is effective in driving these vibrations depends upon the natural frequencies of the vibrational modes, the frequencies of the TMS pulse which drives the vibrations and the damping constants associated with the vibrations. The closer the driving frequencies are to the mechanical vibrational mode frequencies the greater the vibration amplitude of the corresponding mode. Imperfections in the coil geometry and the potting of the windings therefore gives rise to small ballistic and vibrational motions. Motion of the TMS coil, which has a different magnetic susceptibility than both the surrounding air and the subject's head, distorts the static magnetic field across the brain, thereby

deteriorating image quality. Once again, the time course of mechanical vibrations, which depend upon the damping constants of the vibrational modes, will evolve in the period immediately following the TMS pulse.

Given the temporal resolution of MRI, the artifacts produced by leakage currents from the TMS power supply, eddy currents in MRI scanner components, and vibrations of the TMS coil in response to a pulse, are more or less indistinguishable from each other in their effects upon the MRI images. Each will generate signal dropout surrounding the 3D location of the TMS coil. The spatially localized dropout returns to baseline further from the source of the artifact. The time constants can also be expected to overlap. We have attempted to rank the severity of the artifacts by testing on phantoms, leading us to conclude that the leakage current and/or vibration issues is the biggest impediment at present. Changing the proximity of the TMS coil to the magnet had minimal effect on the delay required to obtain clean EPI data. We do not presently have a way to isolate the effects of TMS coil vibration on MRI data, but have found that a delay of 5-10 ms to allow leakage currents and vibrations to abate, is sufficient to permit clean data acquisition.

One final artifact source was considered before we set up our experiment. The application of a TMS pulse of around 1.5 T at the TMS coil surface, combined with a polarizing magnetic field of 3 T, produces an effective field experienced by protons in the vicinity of the TMS coil. Each TMS pulse lasts 250 us, compared to a Larmor frequency at 3 T of over 120 MHz. The TMS pulse duration is more than 30,000 times greater than the precessional period of the spins, suggesting that the magnetization will behave adiabatically and simply follow the applied magnetic field of the TMS pulse. If entirely adiabatic, the magnetization, once exposed to the TMS pulse, should return to its initial state magnetic field associated with the TMS pulse returns smoothly to zero. This return to the prior state depends, however, upon the assumption that any irreversible effects (T1 and T2 decay) upon the magnetization will be negligible during the application of the TMS. Although the time scales associated with the irreversible effects are large compared with the length of the typical TMS pulse, there may be small residual irreversible effects that are large enough to compete with the BOLD signal. We also note that there is a slight asymmetry in the TMS pulse, so that a perfect identity transformation cannot occur. Even so, we predict a minor effect on the TMS experiment, with leakage currents and vibrations likely to dominate in our current hardware.

4.4 Materials and Methods

Concurrent TMS-fMRI was collected at the Henry H. Wheeler Jr. Brain Imaging Center at the University of California, Berkeley and the experiment was approved by the Committee for the Protection of Human Subjects. Subjects participated in two fMRI sessions. The first was a baseline MRI day in which a high resolution T1 scan was acquired using a 12 channel MRI coil. Ten minutes of open-eyes resting state were acquired with the 1 channel MR coil. Subjects were instructed to fixate on a centrally presented fixation cross.

The second session differed between subjects in the location of TMS: either primary motor cortex (M1) or lateral prefrontal cortex (PFC). A different cohort of subjects was acquired for each region of interest. Eight subjects received TMS to M1, and seven subjects received TMS to DLPFC for a total of 15 subject (ages 18 - 29, mean 21.6, standard deviation 2.5). TMS was delivered at 4 different intensities: 40%, 60%, 80% or 100% of motor threshold. The order of TMS intensity was randomized within each block. In each run, subjects received 48 bursts of 4 pulses of TMS at 10Hz separated by 6, 8,10, or 12 seconds. The M1 subjects received 4 runs of TMS-fMRI. The DLPFC subjects received one run of TMS-fMRI.

Magnetic Resonance Imaging

MR data was collected on a Siemens 3T MAGNETOM Trio (Erlangen, Germany). Anatomical data was collected using a 12-channel receive-only head coil using a T_1-weighted magnetization-prepared rapid gradient-echo (MPRAGE) sequence with 192 sagittal slices each 1 mm isotropic voxels, 2.3 second repetition time, interleaved slice acquisition, phase-encoding direction from anterior to posterior, 2.98 millisecond echo time, 9-degree flip angle, and parallel imaging via GeneRalized Autocalibrating Partial Parallel Acquisition (GRAPPA) with an acceleration factor of 2. Alternatively, a subset of subjects were collected on a 12-channel receive-only head coil using a T_1-weighted MPRAGE sequence with 160 sagittal slices each 1 mm isotropic voxels, 50% distance between slices (0.5 mm), 2.3 second repetition time, interleaved slice acquisition, phase-encoding direction from anterior to posterior, 2.98 millisecond echo time, 9-degree flip angle, and parallel imaging via GRAPPA with an acceleration factor of 2. This anatomical scan had a rotated field of view (93.8%) to allow for the neck to be cut in preprocessing without removal of the nose, which is used for registering in neuronavigation.

For functional MRI experiments, we used a custom circularly polarized, receive-only birdcage RF coil (RAPID BioMedical, Rimpar, Germany) because it has a larger inner diameter (256 mm) than standard MR receive coils, and it is open at the back (**Figure 4.1A**). This receive coil is better suited for simultaneous TMS-fMRI as it allows for the TMS coil to be flexibly maneuvered around the scalp, while a TMS coil support can be positioned from the rear (**Figure 4.1A**). We acquired functional data using a T2*-weighted single-shot echo-planar imaging (EPI) sequence with 40 slices of 3.5 x 3.5 x 3.0 mm isotropic voxels, 10% distance between slices, 2 second repetition time (TR), descending slice acquisition order, phase encoding direction anterior-to-posterior, 20 millisecond echo time (TE) , 60-degree flip angle (FA), and fat presaturation. To establish a steady state with respect to spin-lattice relaxation, two dummy volumes of data were obtained at the start of each time series. A further two volumes - the first two recorded volumes - were also excluded from analysis.

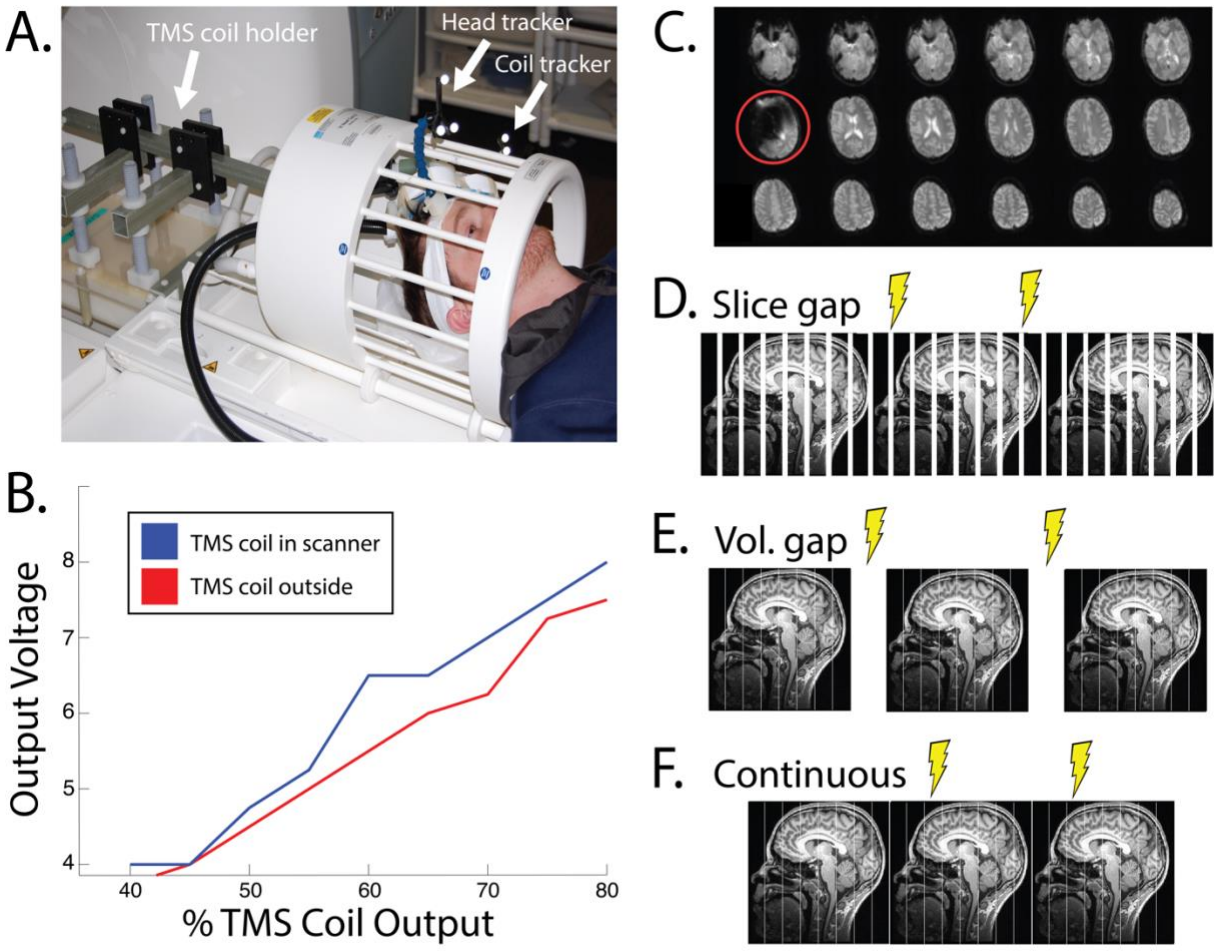

Figure 4.1. Concurrent TMS-fMRI setup. (**A**) Custom built TMS coil holder and neuronavigation head/coil tracker. (**B**) TMS coil output increases inside the bore of the MR scanner. (**C**) Concurrent TMS-fMRI generates considerable noise artifacts. Concurrent TMS can be delivered in imposed gaps between slices (**D**), imposed gaps between slices (**E**), or continuous with fMRI acquisition **(F**).

Transcranial Magnetic Stimulation

Brain stimulation was delivered with the MR-compatible figure-8 MRi-B91 TMS coil produced by MagVenture (Farum, Denmark) with the MagPro X100 booster running software version 7.1.1. The TMS coil is restrained using a custom arm (**Figure 4.1A**). TMS concurrent with fMRI results in significant artifacts to the MRI signal; an example is shown in **Figure 4.1C**. Although the MagVenture system reduces artifacts to some extent, careful experimental design and preprocessing steps are required to clean the fMRI data for statistical analysis. We explain our artifact reduction strategy in more detail below.

During early piloting, we noticed that the intensity of TMS increased when the TMS coil was placed in the bore of the MRI. To test for a systematic difference in the TMS-induced electric field we recorded the electromotive force due to a TMS pulse by using a probe (MagVenture MagProbe) connected to an oscilloscope. The probe was attached to the center of the TMS coil and the electromotive force was recorded within and outside the scanner (**Figure 4.1B**). We found a systematic difference such that TMS within the isocenter of the 3 T magnet produced about a two microvolt increase in intensity relative to the fringe of the magnetic field. This difference corresponds to roughly 5% of MagVenture's coil output. In practice, we treat the intended stimulation intensity as 5% lower within the scanner. We recommend that future researchers be mindful to lower the TMS intensity by a similar proportion to account for this difference in output voltage within the scanner.

MR-compatible Neuronavigation

Rogue Research's BrainSight v2.2.11 (Montreal, Canada) with a Northern Digital Polaris Spectra infrared long-range camera (Waterloo, Ontario, Canada) was used for 3D stereotaxic tracking. In order to accurately target the site of interest, we used neuronavigation within the MRI room itself. The magnetic stand of the infrared long-range camera was replaced with a custom stand constructed of plastic, allowing the camera to be used at the patient bed. The iMac running BrainSight was kept at the doorway to the MRI room and secured to the wall. We custom-designed and 3D-printed head and coil trackers using the dimensions from BrainSight's head and coil trackers for use in the MRI (**Figure 4.1A**). Crucially, the head tracker can be removed from the subject's headband and then reattached within the MR coil. Similarly, the TMS coil tracker can be removed from the TMS coil and reattached within the MR coil. All MR compatible items are marked as such and careful screening was applied to all users and participants. We used a custom-built TMS-coil holder (**Figure 4.1A**) to relieve pressure from the subject's head as the TMS coil exerts scalp pressure for the duration of the TMS-fMRI session. A custom-build mirror system was mounted to the MR coil to provide the subject visibility to the back projected screen (AVOTEC, Stuart, FL, USA), and this included an optional eye-tracking mount (AVOTEC) that was not used in this study.

Real-Time TMS Trigger

In order to establish precision in TMS pulse delivery relative to the MRI sequence, we developed a custom microcontroller-based synchronization system. A Hercules RM42x LaunchPad microcontroller board (Texas Instruments, Dallas, TX, USA) was used to control the synchronization. The microcontroller board was programmed to issue a hardware interrupt upon receiving a synchronization signal from the scanner. For convenience, we utilized TTL pulse programmed to be emitted at the start of each TR period for an EPI time series acquisition. An interrupt service routine then scheduled a signal sent to the trigger port of the TMS unit at user-prescribed time relative to the signal from the scanner. The trigger port of the TMS unit is also hardware interrupt controlled and upon receiving the signal from the microcontroller board

issued a pulse. Since the synchronization signal from the scanner is issued at a fixed position within the scanner sequence for each image volume, and since all signals were detected through hardware interrupts, we were able to obtain completely deterministic synchronization with a guaranteed timing precision of less than one microsecond. Such precision is required for timing the placement of TMS pulses relative to the sequence events of the MRI scanner events and cannot be obtained with user-space code implemented on a standard operating system of a traditional computer. Variability in TMS timing can lead to a number of MR signal artifacts, as discussed in the previous section.

TMS during Continuous Slice Acquisition

Applying TMS pulses simultaneous with any radiofrequency (RF) pulses in the EPI experiment causes pronounced image artifacts in the current volume (**Figure 4.1C**), and perturbs the T_1 steady state for at least three subsequent TR periods. Thus, it is imperative that the TMS pulses and the RF pulses in the EPI time series occur discontinuously. There are two simple ways to avoid simultaneous RF and TMS pulses. Early TMS-fMRI experiments added a gap in acquisition between every slice of a multi-slice EPI volume (**Figure 4.1D**). In this framework, single TMS pulses or bursts of TMS can be delivered at intervals compatible with the gap timing; i.e. one TMS pulse per an integer number of EPI slices. However, this approach decreases the quantity of fMRI data that can be collected in a given period of time. Furthermore, the approach requires millisecond precision of TMS delivery carefully timed to the inter-slice gap. In most recent experiments, a gap in scanning is added between each volume of MR acquisition (**Figure 4.1E**). The gap must be included for every volume of the EPI sequence, rather than before specific volumes only, because we must take care not to perturb the T_1 steady state of the MRI signal. The downside of this framework, once again, is reduced fMRI data collection per unit time. If you wish to deliver a train of TMS pulses at a low frequency, say around 5 Hz, then this method is restrictive in that the volume gap needs to be quite large. For example, delivering 5 pulses of TMS at 5 Hz requires 800 milliseconds, thereby decreasing the EPI sampling duty cycle by nearly 50% for a typical TR of 2.0 seconds. In addition, the TMS is predictably placed within the silent period of the EPI sequence, which may have unforeseen cognitive effects as the subjects are aware of the windows in which TMS will occur. We use a new timing paradigm, depicted in **Figure 4.1E**, that applies TMS pulses during certain "safe" events in the continuous EPI time series. This eliminates the need for a gapped EPI acquisition.

Our timing solution for continuous TMS-fMRI (**Figure 4.1D**) acknowledges all potential sources of artifact (**Table 4.1**). In order to deliver TMS with continuous MR acquisition, we consider three epochs during EPI during which TMS has a different effect on the MR signal ((Bestmann et al., 2012); **Figure 4.2A**). The three epoch are (1) the radiofrequency (RF) stimulation for fat saturation and slice excitation, (2) gradient episodes sampling a k-space plane, and (3) crusher gradients that reset the MR signal between slices or spoil coherence produced by the fat suppression pulse (**Figure 4.2A**). (Note that the crusher and read-out gradients are depicted symbolically in Figure 2A. The actual gradients play out on all three gradient channels and have differing timing depending on intended use.)

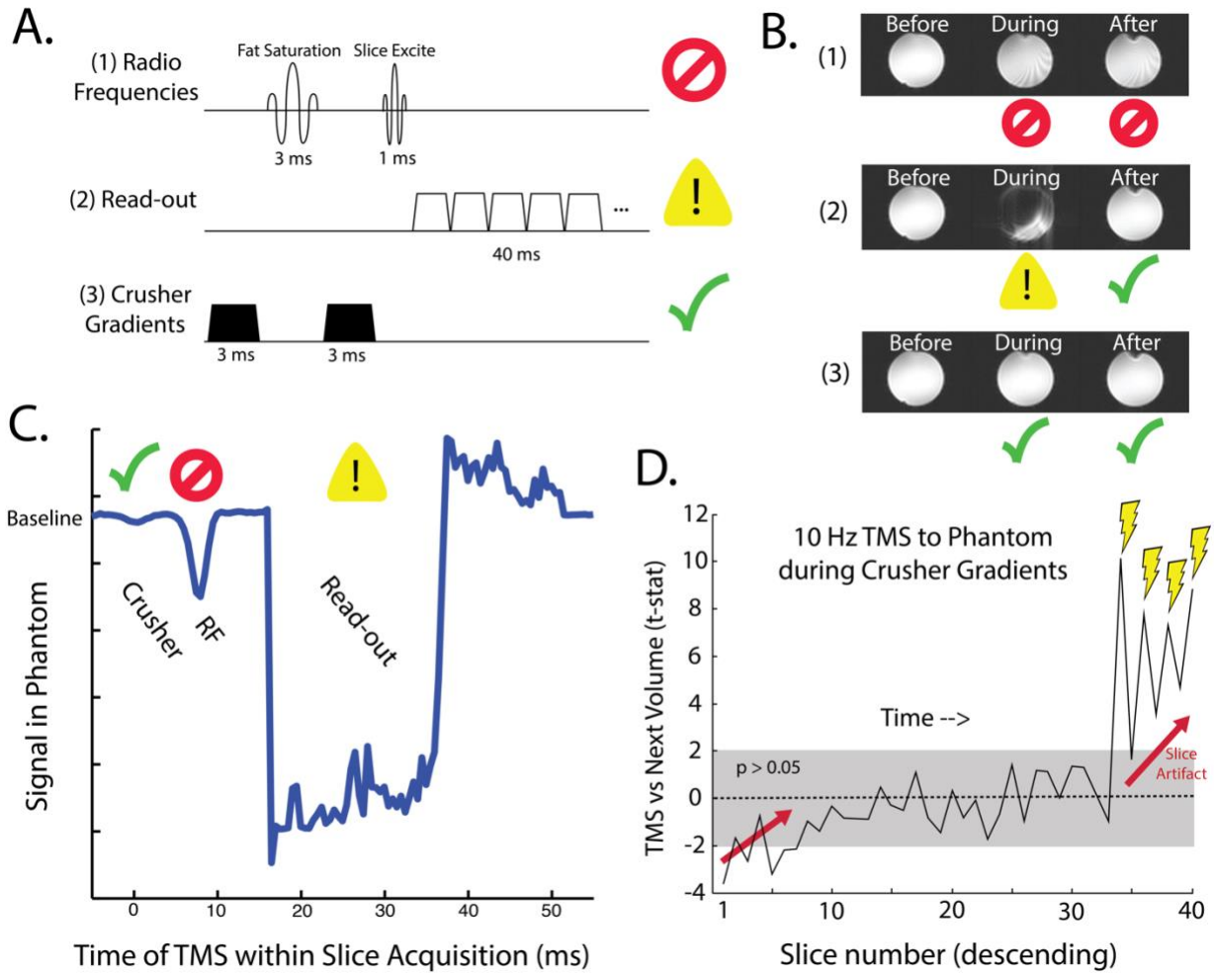

Figure 4.2. Timing of TMS during continuous fMRI. (**A**) Three epochs during fMRI acquisition of a single slice. (**B**) TMS that occurs during each of these three epochs generates different artifacts. (**C**) Stimulation throughout the acquisition of a slice localizes the three epochs. (**D**) TMS during the crusher gradients produces minor slice artifacts that are not visible to the naked eye.

TMS during RF stimulation produces the most pronounced artifacts and should be avoided at all costs. The artifacts affect the current slice acquisition, but also corrupt the MRI signal for multiple subsequent volumes until a steady state is reestablished exponentially with time constant T_1 (**Figure 4.2B**, row 1).

TMS pulses applied during the k-space read-out of the current slice irretrievably corrupts that slice (**Figure 4.2B**, row 2). There is no signal regression that can recover the underlying image. If it becomes imperative to pulse TMS during a k-space read period, we recommend a linear interpolation with the neighboring volumes for that slice. Before any preprocessing steps are applied, the identical slice in the volume before and after can be averaged and substituted to

replace the corrupted slice. Interpolation may induce its own artifact if the subject moves significantly in the volume before or after TMS. If the interpolated slice is an average of data collected from different parts of the brain due to motion, this will induce a spatial and temporal smoothing effect. While TMS during RF stimulation must be avoided, TMS during the read-out gradients should be treated with caution. Given certain experimental designs, such as high frequency rhythmic TMS that exceeds the frequency of slice acquisition, TMS during read-out gradients cannot be avoided. In the case where TMS must be delivered during read-out gradients, we recommend timing the TMS to occur during the acquisition of slices that are of less interest to the particular research question of the experimenter. For example, if the experiment will not analyze fMRI signal in the cerebellum and the MR acquisition includes a few slices in the cerebellum, then temporally align TMS to be delivered during MR acquisition of the most ventral slices. After interpolation of the corrupted slice, there is limited disruption of future volumes.

For a typical $(3\ mm)^3$ spatial resolution, the k-space read-out takes approximately 75% of the total time required per echo planar image; the RF and crusher gradients account for the other 25%. In full k-space sampling (i.e. no partial Fourier), high spatial frequency information is collected first, then low frequency, and finally high frequency again. Given that the majority of signal and contrast in fMRI is acquired during the low frequency center of k-space, it is theoretically possible to align TMS to the end of the read-out period, omit these high frequency k-space lines, and reconstruct a final image using the standard partial Fourier approach. This would recover a usable image, albeit one that is slightly different to the image that would be acquired with a full k-space acquisition in the absence of TMS pulses. Alternatively, the corrupted portion of k-space could be linearly interpolated with k-space from neighboring slices, or from volumes adjacent in time, as noted above. It is also worth noting that targeting stimulation early in the read-out period - immediately following the slice excitation pulse - maximizes the time between the TMS pulse and the RF pulses of the subsequent slice. Thus, if leakage/eddy currents and mechanical vibrations are of concern and it is desired to sample EPI continuously, applying TMS as far as possible from the RF excitation will minimize artifacts.

TMS during crusher gradients provides the least distortion of the MRI signal (**Figure 4.2B** row 3). Crusher gradients are magnetic field episodes that are intended to scramble the phase of unwanted magnetization. There are two principal objectives. Crusher gradients immediately following the fat saturation RF pulse are designed to eliminate coherent fat signal and minimize fat signal at the time of k-space read-out. Crusher gradients at the end of a slice acquisition, following the 2D k-space read-out, are designed to ensure that signal from the prior slice is fully destroyed before exciting and detecting the subsequent slice. (In Figure 2A, we have depicted the second type of crusher gradients as occurring before the fat saturation pulse, for better intuition. In practice, the resetting crusher gradients can be programmed to occur at the start or end of a slice.) The TMS coil produces a biphasic pulsed magnetic field that is asymmetrical in time such that the second lobe is marginally weaker than the first lobe. The biphasic TMS pulse acts as a crusher gradient 6 orders of magnitude greater than the ~40 millitesla crusher gradients imposed by the scanner. Ironically, improved spoiling of unwanted signals from TMS pulses could lead to a situation in which the BOLD signal acquired during TMS-fMRI has improved signal-to-

noise relative to the BOLD signal without TMS, e.g. residual scalp fat signal, which tends to create pronounced N/2 ghosts, might be reduced with TMS. The technical difficulty imposed in targeting the crusher gradients is that these gradients are brief, around 3 milliseconds in the standard Siemens implementation. In order to reliably target the crusher gradient requires sub-millisecond precision timing of TMS. The crusher gradients each precede an RF pulse, which is the most disruptive time to apply TMS. Thus, targeting the crusher periods requires that we pay particular attention to any TMS artifacts that remain once a TMS pulse has been applied. We next consider these TMS "hangover" effects.

If leakage current, eddy currents, or coil vibrations are significant sources of instability, then stimulating during a crusher gradient period may produce local artifacts around the TMS coil that last for several milliseconds, rendering the RF period susceptible to the artifacts. In this scenario, the optimal time for TMS shifts from during crusher gradients to during k-space readout. Without sub-millisecond timing in TMS delivery relative to the MR-sequence, it is safest to align TMS for the center of the read-out period, which lasts for the majority of the slice acquisition. If TMS is successfully delivered during the crusher gradient epoch, then the acquisition will appear to be artifact free upon visual inspection of the data. However, there may still be artifacts in the slices acquired during the delivery of the TMS pulses and related to the TMS coil itself.

Optimizing the TMS-fMRI Timing

We designed our TMS-fMRI protocol to target the crusher gradients that spoil remaining magnetization at the end of each slice acquisition. This crusher gradient is depicted as the first event in the schematic pulse sequence of **Figure 4.2A**. We applied single pulses of TMS with the TMS coil positioned on a plastic bottle of water (Model 8624186 K2285, Siemens, Germany). Using offsets relative to the TTL pulse emitted by the scanner (FIGURE?), we swept through all events of a single EPI slice (**Figure 4.2C**). One hundred pulses of TMS were delivered at 0.5 millisecond offsets relative to the TTL pulse. (The TTL pulse occurs immediately prior to the start of the slice excitation RF pulse.) To ensure the MR signal remained in its steady state, a TMS pulse was applied once every three TR period, for TR=2000 ms. A representation of TMS effects applied through the slice was reconstructed by plotting the mean of the phantom's MR signal (**Figure 4.2C**). The Gaussian shape of the fat saturation pulse is traced out in the artifact profile. While it is not possible to differentiate the slice excitation from the k-space readout immediately following it, it is clear that the artifact level is highest when the signal is greater, i.e. early in the k-space readout.

We next collected a run with a train of 4 pulses of TMS at 10 Hz every 3rd TR, collecting 40 EPI slices in a TR of 2 seconds, in order to evaluate statistically the magnitude of any artifacts remaining following TMS during the crusher gradients. The TMS timing was set such that the last TMS pulse was coincident with the rising edge of the first crusher gradient of the 40th slice. Taking into account the ~10 ms housekeeping events (loop resetting) that arise at the end of each TR, the actual duration of each slice (40 slices in 2 seconds) is ~49.5 ms. A burst of 4 pulses at 10 Hz (100 millisecond inter pulse interval) will drift around 3 milliseconds. To evaluate the impact

of our TMS train on the MR signal, we analyzed the mean of every slice in the volume for which TMS was applied, compared to the mean signal in slices obtained in the TR period immediately after TMS. We used a within factor Student's t-test on the 100 sample points with TMS compared to their subsequent volume. As displayed in **Figure 4.2D**, we found a significant deviation for the slices that received TMS, and this effect culminated throughout the train but returned to baseline within a few slices. Note that these deviations in signal were not visible to the naked eye (**Figure 4.2B**) but are apparent upon statistical testing (**Figure 4.2D**). Also note that the effect of TMS is to generate a small signal increase, not signal drop-out as occurs with TMS during the RF pulses. This effect may be due to increased signal to noise as the TMS pulse acts as an additional crusher gradient. Given this subtle signal change, we advise that experimenters perform linear interpolation over the slices that receive TMS and the slices collected immediately after in the MR sequence.

Removal of TMS Coil Artifacts

The eddy/leakage currents or mechanical vibrations within the TMS coil can perturb the local MR signal for multiple volumes beyond stimulation, sometimes up to 6 seconds (see **Figure 4.3A** for a typical time course of a coil artifact). The coil artifact is not addressed in the majority of studies. We could assume the authors after done due diligence to ensure their BOLD effects are not driven by a coil artifact, but without explicit modeling this false positive cannot be ruled out. Due to the complication of persistent coil artifacts, it is sometimes difficult to validate the efficacy of TMS in the site under the coil and studies may instead focus on distal effects of TMS. The simple empirical question of whether TMS evokes neural activity in the site being stimulated as measured by the BOLD signal has been addressed in a number of studies with mixed success (Bohning et al., 2003). The coil artifact has a characteristic time series and can be explicitly modeled to verify its presence or absence. We suggest that researchers explicitly address the signal under the coil as a proof of principle that TMS has successfully driven neural activity. Our methodology, presented below, characterizes and regresses out the time series associated with the coil artifact when it is present and we provide a standardized means of verifying that the region's BOLD is not driven by a false positive.

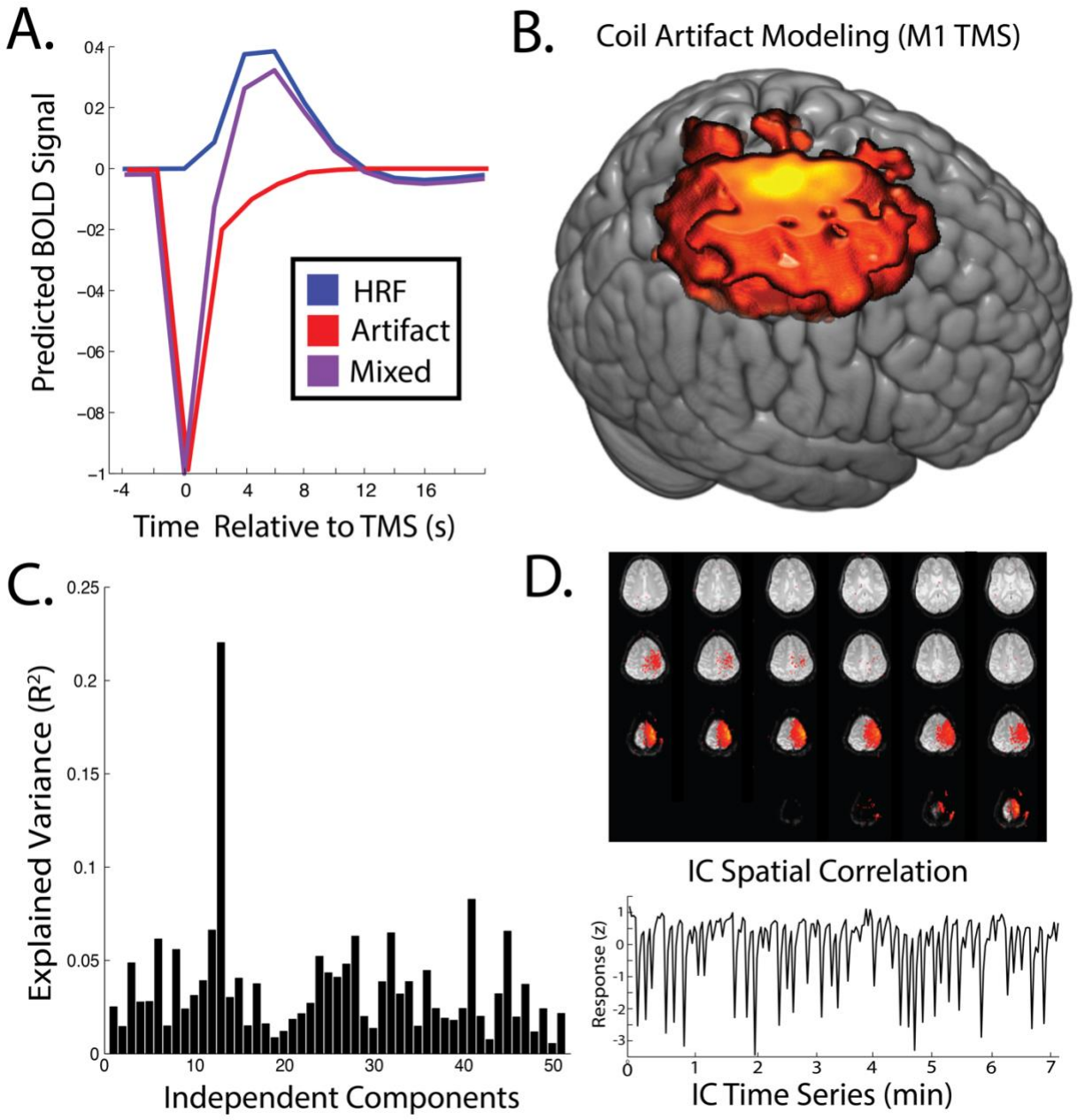

Figure 4.3. Artifacts generated by the TMS coil. (**A**) Time course of a canonical coil artifact, hemodynamic response function, and a mixed signal. (**B**) Inverted gamma function centered on the time of TMS captures the coil artifact. (**C**) Independent Component Analysis (ICA) was used to identify and remove the coil artifact. General linear model (GLM) on each IC time course with the predicted coil artifact. (**D**) Example IC selected from the coil artifact GLM.

In conjunction with running a standard univariate general linear modeling with convolution of the canonical hemodynamic response function, we suggest that experimenters also run a finite impulse response analysis and display the time course of the evoked BOLD signal (**Figure 4.4C**). Given the drop in signal under the coil, a hemodynamic response function modeled at the time of TMS will result in a false positive. As the signal drop returns to baseline, the increase in signal will mimic the rising edge of the hemodynamic response function (**Figure 4.3A**) and standard fMRI analysis pipelines will mistake this pattern as a BOLD response.

When a general linear model was run on data with prominent TMS coil artifacts that treated every TMS pulse as an event convolved with the canonical hemodynamic response, the coil artifact was erroneously identified as a significant BOLD activation. When an inverted gamma function was instead centered around the time of the TMS train to capture the signal drop, the resulting contrast map, as displayed in **Figure 4.3B**, showed a pronounced artifact at the site of stimulation extending into the space above the skull in the location of the TMS coil. A finite impulse response function model reveals that this coil artifact tracks with the intensity of the TMS and lasts for at least 2 volumes (**Figure 4.3A**). In a site of interest under the TMS coil, the artifact is visible in the first 2 volumes dropping and returning to baseline (**Figure 4.4C**).

Given the dramatic effect of coil artifacts, we suggest that researchers conduct quality assurance (QA) scans in which they deliver their TMS pulse sequence to a phantom. The location of the TMS coil should be held constant throughout the QA scans in order to successfully model the MR signal around the TMS coil itself extending into the phantom.

In order to model and remove all TMS coil artifacts driven by eddy/leakage currents or mechanical vibrations, we ran FSL's MELODIC algorithm which decomposes the data into independent components (ICs). Using the time course of each IC, we ran a general linear model that predicted a near-instantaneous signal drop. The explained variance in the time course of the IC by the canonical artifact shape was sufficient for identifying data with TMS coil artifacts (**Figure 4.3C**). After identifying components with a high explained variance from the predicted artifact time course (greater than 10%), we manually inspected the spatial correlation of the component (**Figure 4.3D**). Using this method, we rejected ICs from the data associated with the TMS coil artifact. As discussed later, ICA was successfully able to remove the coil artifact (**Figure 4.4C**).

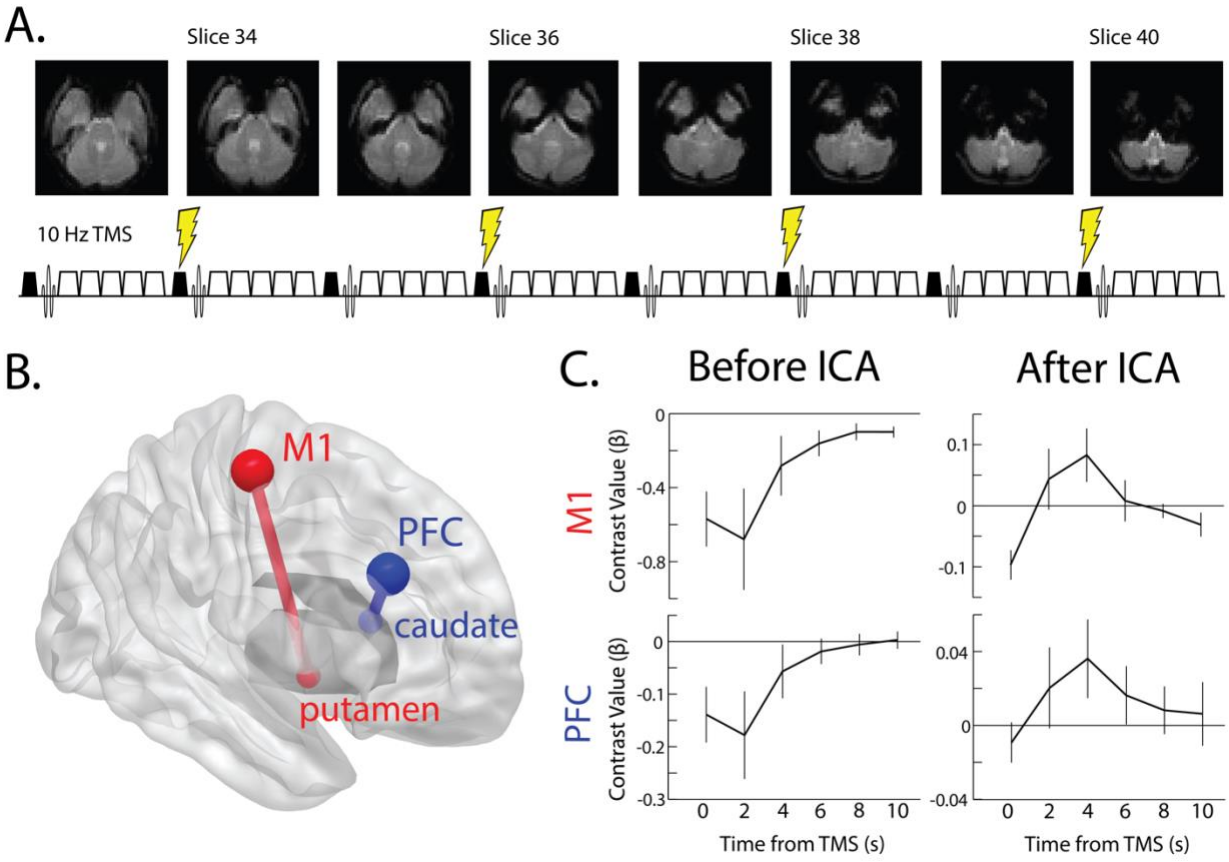

Figure 4.4. Experimental design and coil artifact removal. (**A**) 10 hertz trains of repetitive TMS during the crusher gradients of the most ventral slices. (**B**) TMS to primary motor cortex (M1) and lateral prefrontal cortex (PFC) with anatomical projections to posterior putamen and dorsal caudate, respectively. (**C**) Finite Impulse Response (FIR) model shows the coil artifact in the targeted regions of interest before ICA. After ICA removal, the canonical hemodynamic response function (HRF) is recovered. Error bars are SEM.

Rhythmic TMS Parameters

We chose to use an MR sequence of 40 slices with a 2 second TR. Each slice is collected at 50 millisecond increments. TMS was delivered during the time of least artifact in slice acquisition, and chose a frequency of stimulation that was a multiple of 50 milliseconds (**Figure 4.4A**). We settled on 10 Hz stimulation given the wealth of previous studies using 10 Hz and its proximity to the frequency used by Strafella et al. 2001, 2003.

At the start of the experiment, single pulse TMS was delivered over the right primary motor cortex. Stimulation intensity was increased until TMS reliably evoked a visible twitch in the first dorsal interosseous muscle of the left hand on 5 out of 10 pulses. We used neuronavigation online while calculating the motor threshold. When the motor threshold was found, we marked

the location on the subject's anatomical scan. This region of interest was used for TMS targeting in concurrent TMS-fMRI and for region of interest analysis.

In all subjects, we collected a baseline resting state scan with no TMS. This was used for running a connectivity analysis in order to define in each subject the lateral prefrontal cortex (PFC). Resting state analysis used the preprocessing steps listed above except that the analysis was carried out in subject space and the GLM contained only regressors for motion, mean white matter signal, and mean cerebral spinal fluid signal. The residual images from the GLM are used for the connectivity analysis. The superior precentral sulcus (sPCS) was selected for its known connectivity with lateral PFC and superior intraparietal sulcus (IPS). Furthermore, the right sPCS can be reliably identified by anatomical landmarks: the intersection of the precentral sulcus and the superior frontal sulcus. By running a seed-based resting state connectivity with sPCS we located the coordinates of peak connectivity in PFC and IPS. A seed-based connectivity analysis was also run in IPS and PFC to confirm that these regions form a strongly interconnected functional network (**Figure 4.4B**). This method was established to test hypotheses outside the scope of the current experiment.

TMS-fMRI Session Procedure

BrainSight neuronavigation was used to register the subject's head to a previously acquired structural image. The region of interest was marked directly on the scalp of the subject with a washable marker. The head tracker was detached from the subject's head band and the subject was moved onto the patient bed outside of the scanner. The TMS coil is moved into position with the rough alignment of the marking on the subject's scalp. The coil tracker is attached to the coil in a position that can be easily seen by the infrared camera tracking system. A rough positioning of the coil tracker and subject tracker is acquired within the MR coil before the final stereotaxic registration.

The head and coil trackers were detached from the headband and TMS coil. The TMS coil was calibrated using the newly adjusted coil tracker. The coil tracker was now detached and the coil was attached into the approximate position with the custom-built coil holder system. The subject was placed outside of the scanner on an MRI compatible patient bed. The subject was calibrated again with the position of the headband and flexible head tracker in their approximated alignment. The head tracker was detached and the subject was placed back on the MRI patient bed with their head inside the MR coil. The head tracker was reattached to the headband and coil tracker to the TMS coil. The subject wore earplugs to subdue the sound of TMS and their head was fixated with cushioning that further protected the subject's hearing. The experimenter used BrainSight neuronavigation to make slight adjustments to the coil so that the angle and position of the TMS coil was within a tolerable error limit, less than 5 mm in position and 5 degrees angle.

Before beginning the first session of TMS-fMRI for each subject, we confirmed that the highest intensity of TMS was within a tolerable level and did not produce excessive facial or muscle

twitching. For some subjects, we needed to lower the TMS intensity to match the subject's comfort level and to reduce head motion. The TMS intensity was specifically lower for the lateral PFC site, presumably due to the decreased thickness of the skull and proximity to facial muscles.

fMRI Analysis

After DICOMs are imported, we interpolated over slice artifacts and then used FSL's MELODIC to reject coil artifacts as described above. Preprocessing was carried out in the Statistical Parametric Mapping 12 (SPM12) Toolbox for Matlab, unless otherwise noted. Data was despiked (AFNI), manually reoriented to the anterior commissure, slice time corrected, realigned to the mean functional image using rigid body rotation, coregistered to the anatomical image, and smoothed with a 4 millimeter kernel.

Our first level general linear model had four regressors of interest and eight nuisance regressors. Each train of repetitive TMS was modeled as a boxcar with duration equal to the duration of the TMS burst and convolved with the hemodynamic response function. The four regressors of interest were the four intensities of TMS (40%, 60%, 80%, and 100% of motor threshold). Of the eight nuisance regressors, six modeled motion generated by SPM's realignment for the three spatial dimensions and three angles of rotation. The other two nuisance regressors quantified the mean signal in physiological system of non-interest global white matter and cerebral spinal fluid. These regressors were generated by calculating the mean signal within a mask generated by tissue estimations from SPM12's segmentation.

We defined our region of interest (ROI) in posterior putamen and dorsal caudate based on two previous studies that applied repetitive TMS to M1 and PFC, respectively, and found the maximum amount extracellular dopamine release (as measured by a reduction in [^{11}C]raclopide signal in PET scanning) (Strafella et al., 2001; 2003) ;**Figure 4.4B**). A 6 mm diameter ROI was defined with the center of mass at (34, 3, -5) for putamen, and (13, 15, 11) for caudate using the MarsBaR toolbox ((Brett et al., 2002), http://marsbar.sourceforge.net/). These regions were defined in the Montreal Neurological Institute (MNI) normalized space.

After the GLM was run for each subject, the contrast images were normalized into MNI space for group level analysis. We extracted the mean evoked BOLD activity from the univariate analysis for all ROIs: M1, PFC, caudate, and putamen. The contrast images of interest were the four TMS intensities and a contrast image for the parametric effect of TMS intensity. We ran a two-way analysis of variable (ANOVA) with a between subject factor for TMS to M1 or PFC and a within subject factor for the BOLD signal in the regions of interest: either M1 and PFC or putamen and caudate.

A finite impulse response (FIR) model was run to confirm that our BOLD effects were not driven by scanner artifacts. The FIR model was chosen to capture the 12 second period following TMS in six gamma functions, each lasting the duration of a single TR, 2 seconds. Therefore, the GLM

for the FIR model has 24 regressors of interest six for each of the four TMS intensities and the eight nuisance regressors used in the univariate GLM.

4.5 Results

We hypothesized that TMS to M1 would evoke a BOLD response in M1 and TMS to PFC would evoke a BOLD response in PFC. To test this hypothesis, we ran a two-way analysis of variance (ANOVA) with the between subject factor of the site of TMS by the within subject factor of BOLD signal in the targeted region and the non-targeted region. We found a weak interaction between TMS site and the BOLD signal of the targeted versus non-targeted site ($F(1,13) = 2.70$, $p = 0.125$, $\eta^2 = .21$). In particular, we hypothesized that TMS at 100% of motor threshold would result in the largest effects on BOLD signal in the stimulated region. A two-way ANOVA for only the highest amplitude TMS revealed the same interaction with a stronger effect ($F(1,13) = 6.67$, $p = 0.023$, $\eta^2 = .51$). Additionally, there was a main effect of the targeted regions ($F(1,13) = 3.534$, $p = 0.083$, $\eta^2 = .27$), because M1 was activated by TMS to both M1 ($t(7) = 2.74$, $p = 0.029$, $d = 0.97$; **Figure 4.5A**) and PFC (($t(7) = 1.93$, $p = 0.10$, $d= 0.73$; **Figure 4.5B**) whereas PFC was only activated by TMS to PFC ($t(6) = 2.55$, $p = 0.043$, $d = 0.97$; **Figure 4.5B**) but not by TMS to M1 ($t(6) = -0.0045$, $p = 0.99$, $d = 0.002$; **Figure 4.5A**). These findings confirm our hypothesis that TMS to a region increases the BOLD signal in the targeted location. Furthermore, our findings are suggestive of a cortical hierarchy in which PFC occupies a higher location (Verstynen et al., 2012). The defining characteristic of a hierarchy is an asymmetry in projections such that higher regions project to lower regions but the lower regions do not project to the higher regions (Badre and D'Esposito, 2009). Our results suggest a functional hierarchy in that TMS to PFC activated both PFC and M1, whereas TMS to M1 did not activate PFC.

We hypothesized that TMS to M1 would evoke a BOLD signal response in the anatomically connected site in posterior putamen whereas TMS to PFC would primarily evoke a BOLD signal response in the dorsal caudate nucleus. To test this hypothesis, we ran a two-way ANOVA with the between subject factor of the site of TMS by the within subject factor of the parametric BOLD signal as TMS intensity increases in the striatal sites. We found an interaction between TMS site and striatal site ($F(1,13) = 5.92$, $p = 0.032$, $\eta^2 = .49$). TMS to M1 did not show a significant parametric BOLD signal increase in putamen ($t(7) = 1.55$, $p = 0.17$, $d = 0.55$; **Figure 4.5C**) or caudate ($t(7) = -0.78$, $p = 0.46$, $d = 0.28$); however, the parametric response was greater in putamen than caudate ($t(7) = 2.20$, $p = 0.064$, $d = 0.78$) and the highest amplitude of TMS output showed a significant BOLD signal response in putamen ($t(7) = 3.04$, $p = 0.019$, $d = 1.08$), but was negative in the caudate ($t(7) = -2.05$, $p = 0.08$, $d = 0.72$). TMS to PFC showed a significant parametric increase in BOLD signal in both putamen ($t(6) = 2.70$, $p = 0.036$, $d = 1.02$; **Figure 4.5D**) and caudate ($t(6) = 3.20$, $p = 0.019$, $d = 1.21$). As hypothesized, TMS to M1 preferentially activated the posterior putamen whereas TMS to PFC preferentially activated the dorsal caudate nucleus. In support of hierarchical anatomy, TMS to M1 spread only to the putamen whereas TMS to PFC spread to both caudate and putamen.

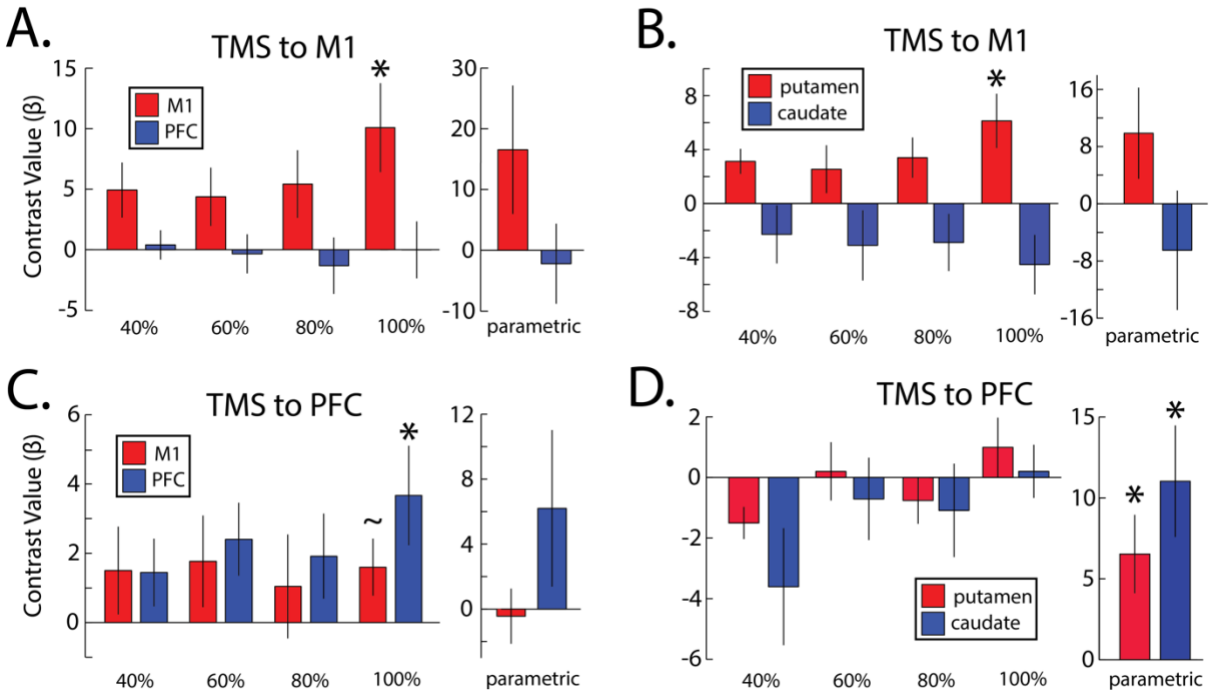

Figure 4.5. Experimental results. BOLD response upon TMS to M1 (**A**,**B**) and PFC (**C**,**D**). Contrast values from univariate analysis with increasing stimulus intensity at 40%, 60%, 80%, and 100% of motor threshold and the parametric increase with stimulus intensity in M1/PFC (**A**,**C**) and putamen/caudate (**B**,**D**). Error bars are SEM. * $p < 0.05$, ~ $p < 0.1$

4.6 Discussion

The methodological framework established in this experiment provides critical groundwork for replicating the TMS-fMRI environment in other labs. Our results demonstrate that given the proper considerations, TMS-fMRI can produce relatively artifact free data that reliably demonstrates activation in the targeted region. Experimenters should guarantee sub-millisecond precision in their TMS timing relative to their MR sequence and quantify the degree to which artifacts are present in a phantom. Furthermore, quality assurance TMS-fMRI scans should be run throughout the experiment to ensure that TMS coil performance does not drift from optimal. Experimenters should interpolate over the MR slices at which TMS is delivered and the subsequent slice. Before applying a preprocessing pipeline, independent component analysis should be run to remove independent components that correlate significantly with an instantaneous signal dropout at the time of TMS. Significant BOLD responses from TMS should be confirmed to not be driven by artefactual signal dropout by running a finite impulse response model of the assumed hemodynamic response function. Evoked activity should be confirmed to begin at baseline levels and rise according to the traditional HRF response.

Our results provide causal evidence that TMS activates the region under the coil and the regions in basal ganglia with single synaptic anatomical connections. We further find evidence for a

rostro-caudal hierarchy in the frontal cortex characterized by asymmetrical projections towards more posterior sites (Verstynen et al., 2012). TMS to PFC spread not only to the dorsal caudate nucleus but also to the posterior putamen and primary motor cortex.

TMS concurrent with fMRI provides critical insight into the efficacy and spread of TMS. Noninvasive brain stimulation studies are known to exhibit inter-subject variability (López-Alonso et al., 2014). Quantifying the degree to which TMS is able to evoke activity in the targeted region provides a potential avenue for quantifying the degree to which TMS is efficacious.

Chapter 5

Conclusions and Future Directions

In this dissertation, I have provided causal evidence that beta and gamma frequency neural oscillations carry top-down and bottom-up attention signals (**Ch. 2**). Theta frequency neural oscillations are causally involved in the reactivation of working memory representations and alpha frequency neural oscillations are causally involved in actively suppressing irrelevant working memory representations (**Ch. 3**). Finally, I developed a methodology for concurrent TMS-fMRI that builds from previous methods and establishes a standardized approach for future experimenters (**Ch. 4**).

The projects described in this thesis have spurned a multitude of experiments that are either underway or nearly complete. Given my interest in neural oscillations, I conducted an electroencephalography (EEG) experiment that studies the neural basis of cognitive control. Our task involved two dimensions of manipulation: the set size of rules that subjects must learn and the level of abstraction involved in those rules. We hypothesized that distinct neural oscillatory mechanisms would underlie the cognitive processes required by this task. As hypothesized, beta frequency oscillations were essential for the higher abstraction rules. Similar to the beta oscillations manipulated by TMS in **Ch. 2** that guided top-down attention, the higher abstraction rules employ more top-down attention to implement the multi-stage goal-directed policies. Similar to the theta oscillations manipulated by TMS in **Ch. 3** that reactivated working memory representations, the increased set size of rules to be maintained in long-term memory increased theta oscillatory activity. This double dissociation extends the literature surrounding beta and theta frequency neural oscillations into the domain of policy abstraction and hierarchical cognitive control (Badre, 2008). Future directions involve concurrent fMRI with rhythmic TMS (method developed in **Ch. 4**) in beta and theta frequency to probe the network level organization of theta and beta rhythms. We hypothesize that the theta frequency TMS will activate a hippocampal bottom-up stimulus processing network (Hsieh and Ranganath, 2014), whereas beta frequency TMS will activate a frontal-parietal attention network (Antzoulatos and Miller, 2014) and subcortical projections in the basal ganglia (Brittain and Brown, 2014).

Using the methods established in **Ch. 4**, I have collected a dataset in which multiple regions of the brain are stimulated in different frequency bands. If neural oscillations are a mechanism of information transfer between regions and different types of information occupy different bands in the frequency domain, then stimulation of a single region in different frequency bands should activate separable brain network associated with those frequency bands (Rosanova et al., 2009).

Further utilizing the methods established in **Ch. 4** and a follow up to the frequency stimulation from **Ch. 2**, I have run an experiment in which subject perform a delayed match-to-sample task. This working memory task has been shown to engage both beta and gamma frequency neural

oscillations (Lundqvist et al., 2016). Preliminary results show that subjects display a disruption to working memory performance from both beta and gamma frequency TMS. However, the neural basis of this disruption differs depending on the frequency of stimulation. Beta frequency stimulation loads on the frontal parietal network whereas gamma frequency stimulation loads particularly on V4, a visual processing region. These early results support our findings in **Ch. 2** that stimulation in beta frequency spreads throughout a top-down attention network while gamma frequency stimulation spreads to those regions most sensitive to bottom-up information.

Finally, I will be beginning a post-doctoral fellowship in Flavio Fröhlich's lab at University of North Carolina, Chapel Hill. In addition to further investigating the causal role of neural oscillations in cognition, I will be working with populations with psychiatric illness. In particular, the success of TMS for the treatment of depression (Perera et al., 2016) still may suffer from suboptimal stimulation parameter decisions. For example, stimulation at the intrinsic frequency of a subject's naturally occurring brain rhythm has been shown to maximize the efficacy of stimulation (Romei et al., 2016a). Furthermore, the endogenous activity of a region at the time of TMS may alter, or even reverse, the effect of TMS (**Ch. 3**). I propose that clients passively receiving brain stimulation may not be utilizing the full impact of stimulation. Alternatively, clients actively engaged in cognitive behavioral therapy with the simultaneous application of noninvasive brain stimulation might experience a constructive interference between the interventions. If the noninvasive brain stimulation is intended to alter the neural circuitry responsible for pathological cognitive processing, engaging healthy cognitive and behavioral modes concurrent with the brain stimulation could interact to reinforce or build positive neural circuitry.

In conclusion, the thesis work presented here represents a substantial extension of human understanding on the neural oscillatory basis of cognition. Future research will build off this foundational work with the potential to augment established methods for the treatment of psychiatric illness.

References

Albouy P, Weiss A, Baillet S, Zatorre RJ (2017) Selective Entrainment of Theta Oscillations in the Dorsal Stream Causally Enhances Auditory Working Memory Performance. Neuron 94:1–14.

Alekseichuk I, Turi Z, de Lara GA, Antal A, Paulus W (2016) Spatial Working Memory in Humans Depends on Theta and High Gamma Synchronization in the Prefrontal Cortex. Current Biology 26:1–10.

Antzoulatos EG, Miller EK (2014) Increases in Functional Connectivity between Prefrontal Cortex and Striatum during Category Learning. Neuron 83:216–225.

Antzoulatos EG, Miller EK (2016) Synchronous beta rhythms of frontoparietal networks support only behaviorally relevant representations. eLife:1–22.

Badre D (2008) Cognitive control, hierarchy, and the rostro–caudal organization of the frontal lobes. Trends in Cognitive Sciences 12:193–200.

Badre D, D'Esposito M (2009) Is the rostro-caudal axis of the frontal lobe hierarchical? Nat Rev Neurosci 10:659–669.

Bastos AM, Loonis R, Kornblith S, Lundqvist M, Miller EK (2018) Laminar recordings in frontal cortex suggest distinct layers for maintenance and control of working memory. Proceedings of the National Academy of Sciences 63:201710323–201710326.

Bastos AM, Vezoli J, Bosman CA, Schoffelen J-M, Oostenveld R, Dowdall JR, De Weerd P, Kennedy H, Fries P (2015) Visual Areas Exert Feedforward and Feedback Influences through Distinct Frequency Channels. Neuron 85:390–401.

Bestmann S, Ruff CC, Driver J, Blankenburg F (2012) Concurrent TMS and functional magnetic resonance imaging: methods and current advances. Oxford University Press.

Bohning D (1999) A Combined TMS/fMRI Study of Intensity-Dependent TMS Over Motor Cortex. :1–10.

Bohning DE, Shastri A, Lomarev MP, Lorberbaum JP, Nahas Z, George MS (2003) BOLD-fMRI response vs. transcranial magnetic stimulation (TMS) pulse-train length: Testing for linearity. J Magn Reson Imaging 17:279–290.

Börgers C, Kopell N (2007) Gamma oscillations and stimulus selection. Neural Computation 20:383–414.

Brett M, Anton J-L, Valabregue R, Poline J-B (2002) Region of interest analysis using an SPM toolbox. Internation Conferance on Functional Mapping of the Human Brain:1–1.

Brittain J-S, Brown P (2014) Oscillations and the basal ganglia: Motor control and beyond. NeuroImage 85:637–647.

Bungert A (2010) TMS combined with fMRI Bowtell R, ed. :1–253.

Buschman TJ, Miller EK (2007) Top-Down Versus Bottom-Up Control of Attention in the Prefrontal and Posterior Parietal Cortices. Science 315:1860–1862.

Buschman TJ, Miller EK (2009) Serial, Covert Shifts of Attention during Visual Search Are Reflected by the Frontal Eye Fields and Correlated with Population Oscillations. Neuron 63:386–396.

Buzsáki G (2002) Theta Oscillations in the Hippocampus Review. Neuron 33:325–340.

Buzsáki G (2006) Rhythms of the Brain. Oxford University Press.

Buzsáki G, Anastassiou CA, Koch C (2012) The origin of extracellular fields and currents — EEG, ECoG, LFP and spikes. Nat Rev Neurosci 13:1–14.

Cameron IGM, Riddle JM, D'Esposito M (2015) Dissociable Roles of Dorsolateral Prefrontal Cortex and Frontal Eye Fields During Saccadic Eye Movements. Front Hum Neurosci 9:624–14.

Canolty RT, Knight RT (2010) The functional role of cross-frequency coupling. Trends in Cognitive Sciences 14:506–515.

Chanes L, Quentin R, Tallon-Baudry C, Valero-Cabre A (2013) Causal Frequency-Specific Contributions of Frontal Spatiotemporal Patterns Induced by Non-Invasive Neurostimulation to Human Visual Performance. Journal of Neuroscience 33:5000–5005.

Corbetta M, Shulman GL (2002) Control of goal-directed and stimulus-driven attention in the brain. Nat Rev Neurosci 3:201–215.

Cox RW (1996) AFNI: Sofware for Analysis and Visualization of Functional Resonance Neuroimages. Computers and Biomedical Research 29:162–173.

Crespo-Garcia M, Pinal D, Cantero JL, Díaz F, Zurrón M, Atienza M (2013) Working Memory Processes Are Mediated by Local and Long-range Synchronization of Alpha Oscillations. Journal of Cognitive Neuroscience 25:1343–1357.

D'Esposito M, Postle BR (2015) The Cognitive Neuroscience of Working Memory. Annu Rev Psychol 66:115–142.

Dai Z, de Souza J, Lim J, Ho PM, Chen Y, Li J, Thakor N, Bezerianos A, Sun Y (2017) EEG Cortical Connectivity Analysis of Working Memory Reveals Topological Reorganization in Theta and Alpha Bands. Front Hum Neurosci 11:e30017–13.

Dale A (1999) Optimal Experimental Design for Event-Related fMRI. Hum Brain Mapp 8:109–114.

Donner TH, Kettermann A, Diesch E, Ostendorf F, Villringer A, Brandt SA (2002) Visual Feature and Conjunction Searches of Equal Difficulty Engage Only Partially Overlapping Frontoparietal Networks. NeuroImage 15:16–25.

Draganski B, Kherif F, Kloppel S, Cook PA, Alexander DC, Parker GJM, Deichmann R, Ashburner J, Frackowiak RSJ (2008) Evidence for Segregated and Integrative Connectivity Patterns in the Human Basal Ganglia. Journal of Neuroscience 28:7143–7152.

Engel AK, Fries P (2010) Beta-band oscillations - signalling the status quo? Current Opinion in Neurobiology 20:156–165.

Fries P (2015) Rhythms for Cognition: Communication through Coherence. Neuron 88:220–235.

Fries P, Reynolds J, Rorie A, Desimone R (2001) Modulation of Oscillatory Neuronal Synchronization by Selective Visual Attention. Science 291:1560–1563.

Fröhlich F, McCormick DA (2010) Endogenous Electric Fields May Guide Neocortical Network Activity. Neuron 67:129–143.

Gazzaley A, Nobre AC (2012) Top-down modulation: bridging selective attention and working memory. Trends in Cognitive Sciences 16:128–134.

Grefkes C, Fink GR (2005) The functional organization of the intraparietal sulcus in humans and monkeys. Journal of Anatomy 207:3–17.

Gregoriou GG, Gotts SJ, Zhou H, Desimone R (2009) High-Frequency, Long-Range Coupling Between Prefrontal and Visual Cortex During Attention. Science 324:1207–1210.

Griffin I, Nobre AC (2003) Orienting Attention to Locations in Internal Representations. Journal of Cognitive Neuroscience 15:1176–1194.

Hanslmayr S, Matuschek J, Fellner M-C (2014) Entrainment of Prefrontal Beta Oscillations Induces an Endogenous Echo and Impairs Memory Formation. Current Biology 24:904–909.

Herrmann CS, Strüber D, Helfrich RF, Engel AK (2016) EEG oscillations: From correlation to causality. International Journal of Psychophysiology 103:12–21.

Hsieh L-T, Ranganath C (2014) Frontal midline theta oscillations during working memory maintenance and episodic encoding and retrieval. NeuroImage 85:721–729.

Huang Y-Z, Edwards MJ, Rounis E, Bhatia KP, Rothwell JC (2005) Theta Burst Stimulation of the Human Motor Cortex. Neuron 45:201–206.

Jarbo K, Verstynen TD (2015) Converging Structural and Functional Connectivity of Orbitofrontal, Dorsolateral Prefrontal, and Posterior Parietal Cortex in the Human Striatum. Journal of Neuroscience 35:3865–3878.

Jaušovec N, Jaušovec K (2014) Increasing working memory capacity with theta transcranial alternating current stimulation (tACS). Biological Psychology 96:42–47.

Jensen O, Lisman JE (1996) Theta/Gamma Networks with Slow NMDA Channels Learn Sequences and Encode Episodic Memory: Role of NMDA Channels in Recall. Learning Memory 3:264–278.

Johnson EL, Dewar CD, Solbakk A-K, Endestad T, Meling TR, Knight RT (2017) Bidirectional Frontoparietal Oscillatory Systems Support Working Memory. Current Biology 27:1–12.

Jokisch D, Jensen O (2007) Modulation of Gamma and Alpha Activity during a Working Memory Task Engaging the Dorsal or Ventral Stream. Journal of Neuroscience 27:3244–3251.

Klimesch W (1999) EEG alpha and theta oscillations reflect cognitive and memory performance: a review and analysis. Brain Research Reviews 29:169–195.

Klimesch W (2012) Alpha-band oscillations, attention, and controlled access to stored information. Trends in Cognitive Sciences 16:606–617.

Klimesch W, Doppelmayr M, Russegger H, Pachinger T (1996) Theta band power in the human scalp EEG and the encoding of new information. Neuroreport 7:1235–1240.

Klimesch W, Schimke D, Ripper B (1997) Theta synchronization and alpha desynchronization in a memory task. Psychophysiology 34:169–176.

Kornblith S, Buschman TJ, Miller EK (2016) Stimulus Load and Oscillatory Activity in Higher Cortex. Cerebral Cortex 26:3772–3784.

Liebe S, Hoerzer GM, Logothetis NK, Rainer G (2012) Theta coupling between V4 and prefrontal cortex predicts visual short-term memory performance. Nature Publishing Group 15:456–462.

Lisman JE, Jensen O (2013) Perspective. Neuron 77:1002–1016.

López-Alonso V, Cheeran B, Río-Rodríguez D, Fernández-del-Olmo M (2014) Inter-individual Variability in Response to Non-invasive Brain Stimulation Paradigms. Brain Stimulation 7:372–380.

Lundqvist M, Rose J, Herman P, Brincat SL, Buschman TJ, Miller EK (2016) Gamma and Beta Bursts Underlie Working Memory. Neuron 90:1–24.

Marshall TR, O'Shea J, Jensen O, Bergmann TO (2015) Frontal Eye Fields Control Attentional

Modulation of Alpha and Gamma Oscillations in Contralateral Occipitoparietal Cortex. Journal of Neuroscience 35:1638–1647.

Michalareas G, Vezoli J, van Pelt S, Schoffelen J-M, Kennedy H, Fries P (2016) Alpha-Beta and Gamma Rhythms Subserve Feedback and Feedforward Influences among Human Visual Cortical Areas. Neuron 89:384–397.

Mochizuki H, Franca M, Huang Y-Z, Rothwell JC (2005) The role of dorsal premotor area in reaction task: comparing the “virtual lesion” effect of paired pulse or theta burst transcranial magnetic stimulation. Experimental Brain Research 167:414–421.

Moran RJ, Campo P, Maestu F, Reilly RB, Dolan RJ, Strange BA (2010) Peak Frequency in the Theta and Alpha Bands Correlates with Human Working Memory Capacity. Front Hum Neurosci 4:1–12.

Myers NE, Stokes MG, Nobre AC (2017) Prioritizing Information during Working Memory: Beyond Sustained Internal Attention. Trends in Cognitive Sciences 21:449–461.

O'Shea J, Johansen-Berg H, Trief D, Göbel S, Rushworth MFS (2007) Functionally Specific Reorganization in Human Premotor Cortex. Neuron 54:479–490.

Pascual-Leone A, Walsh V, Rothwell JC (2000) Transcranial magnetic stimulation in cognitive neuroscience – virtual lesion, chronometry, and functional connectivity Alvaro Pascual-Leone. Current Opinion in Neurobiology 10:232–237.

Perera T, George MS, Grammer G, Janicak PG, Pascual-Leone A, Wirecki TS (2016) The Clinical TMS Society Consensus Review and Treatment Recommendations for TMS Therapy for Major Depressive Disorder. Brain Stimulation 9:336–346.

Poch C, Campo P, Barnes GR (2014) Modulation of alpha and gamma oscillations related to retrospectively orienting attention within working memory. European Journal of Neuroscience 40:2399–2405.

Poch C, Capilla A, Hinojosa JA, Campo P (2017) Selection within working memory based on a color retro-cue modulates alpha oscillations. Neuropsychologia 106:133–137.

Poch C, Valdivia M, Capilla A, Hinojosa JA, Campo P (2018) Suppression of no-longer relevant information in Working Memory_ An alpha-power related mechanism? Biological Psychology 135:112–116.

Quentin R, Elkin Frankston S, Vernet M, Toba MN, Bartolomeo P, Chanes L, Valero-Cabré A (2016) Visual Contrast Sensitivity Improvement by Right Frontal High-Beta Activity Is Mediated by Contrast Gain Mechanisms and Influenced by Fronto-Parietal White Matter Microstructure. Cerebral Cortex 26:2381–2390.

Reinhart R (2017) Disruption and rescue of interareal theta phase coupling and adaptive

behavior. Proceedings of the National Academy of Sciences 114:11542–11547.

Reuter-Lorenz PA, Hughes HC, Fendrich R (1991) The reduction of saccadic latency by prior offset of the fixation point: An analysis of the gap effect. Perception Psychophysics 49:167–175.

Richter CG, Thompson WH, Bosman CA, Fries P (2017) Top-down beta enhances bottom-up gamma. Journal of Neuroscience:3771–16–41.

Robinson DA, Fuchs AF (1969) Eye Movements Evoked by Stimulation of Frontal Eye Fields. Journal of Neurophysiology 32:637–648.

Romei V, Bauer M, Brooks JL, Economides M, Penny W, Thut G, Driver J, Bestmann S (2016a) Causal evidence that intrinsic beta-frequency is relevant for enhanced signal propagation in the motor system as shown through rhythmic TMS. NeuroImage 126:120–130.

Romei V, Driver J, Schyns PG, Thut G (2011) Rhythmic TMS over Parietal Cortex Links Distinct Brain Frequencies to Global versus Local Visual Processing. Current Biology 21:334–337.

Romei V, Gross J, Thut G (2010) On the Role of Prestimulus Alpha Rhythms over Occipito-Parietal Areas in Visual Input Regulation: Correlation or Causation? Journal of Neuroscience 30:8692–8697.

Romei V, Thut G, Silvanto J (2016b) Information-Based Approaches of Noninvasive Transcranial Brain Stimulation. Trends in Neurosciences 39:782–795.

Rosanova M, Casali A, Bellina V, Resta F, Mariotti M, Massimini M (2009) Natural Frequencies of Human Corticothalamic Circuits. Journal of Neuroscience 29:7679–7685.

Rose EJ, Ebmeier KP (2006) Pattern of impaired working memory during major depression. Journal of Affective Disorders 90:149–161.

Rouder JN, Morey RD, Morey CC, Cowan N (2011) How to measure working memory capacity in the change detection paradigm. Psychon Bull Rev 18:324–330.

Roux F, Uhlhaas PJ (2014) Working memory and neural oscillations: alpha–gamma versus theta–gamma codes for distinct WM information? Trends in Cognitive Sciences 18:16–25.

Sauseng P, Griesmayr B, Freunberger R, Klimesch W (2010) Control mechanisms in working memory: A possible function of EEG theta oscillations. Neuroscience and Biobehavioral Reviews 34:1015–1022.

Sauseng P, Klimesch W, Heise KF, Gruber WR, Holz E, Karim AA, Glennon M, Gerloff C, Birbaumer N, Hummel FC (2009) Brain Oscillatory Substratesof Visual Short-Term Memory Capacity. Current Biology 19:1846–1852.

Schall JD, Morel A, King D, Bullier J (1995) Topography of Visual Cortex Connections with Frontal Eye Field in Macaque: Convergence and Segregation of Processing Streams. Journal of Neuroscience 15:4464–4487.

Shadlen M, Movshon JA (1999) Synchrony Unbound: Review A Critical Evaluation of the Temporal Binding Hypothesis. Neuron 24:67–77.

Shulman GL (2003) Quantitative Analysis of Attention and Detection Signals During Visual Search. Journal of Neurophysiology 90:3384–3397.

Siegel M, Donner TH, Engel AK (2012) Spectral fingerprints of large-scale neuronal interactions. Nat Rev Neurosci 13:121–134.

Silver MA, Kastner S (2009) Topographic maps in human frontal and parietal cortex. Trends in Cognitive Sciences 13:488–495.

Souza AS, Oberauer K (2016) In search of the focus of attention in working memory: 13 years of the retro-cue effect. Attention, Perception, & Psychophysics 78:1–22.

Stanley D, Roy J, Aoi M, Kopell N, Miller EK (2016) Low-Beta Oscillations Turn Up the Gain During Category Judgements. Cerebral Cortex:1–15.

Stoll FM, Wilson CRE, Faraut MCM, Vezoli J, Knoblauch K, Procyk E (2016) The Effects of Cognitive Control and Time on Frontal Beta Oscillations. Cerebral Cortex 26:1715–1732.

Strafella AP, Paus T, Barrett J, Dagher A (2001) Repetitive Transcranial Magnetic Stimulation of the Human Prefrontal Cortex Induces Dopamine Release in the Caudate Nucleus. Journal of Neuroscience 21:1–4.

Strafella AP, Paus T, Fraraccio M, Dagher A (2003) Striatal dopamine release induced by repetitive transcranial magnetic stimulation of the human motor cortex. Brain 126:2609–2615.

Sutherland GR, McNaughton B (2000) Memory trace reactivation in hippocampal and neocortical neuronal ensembles. Current Opinion in Neurobiology 10:180–186.

Thut G (2011) Entrainment of perceptually relevant brain oscillations by non‐invasive rhythmic stimulation of the human brain. :1–10.

Thut G, Veniero D, Romei V, Miniussi C, Schyns P, Gross J (2011) Rhythmic TMS Causes Local Entrainment of Natural Oscillatory Signatures. Current Biology 21:1176–1185.

Vernet M, Quentin R, Chanes L, Mitsumasu A, Valero-Cabré A (2014) Frontal eye field, where art thou? Anatomy, function, and non-invasive manipulation of frontal regions involved in eye movements and associated cognitive operations. Front Integr Neurosci 8:1–24.

Verstynen TD, Badre D, Jarbo K, Schneider W (2012) Microstructural organizational patterns in the human corticostriatal system. Journal of Neurophysiology 107:2984–2995.

Wagner T, Rushmore J, Eden U, Valero-Cabré A (2009a) Biophysical foundations underlying TMS: Setting the stage for an effective use of neurostimulation in the cognitive neurosciences. CORTEX 45:1025–1034.

Wagner T, Rushmore J, Eden U, Valero-Cabré A (2009b) Biophysical foundations underlying TMS: Setting the stage for an effective use of neurostimulation in the cognitive neurosciences. CORTEX 45:1025–1034.

Wallis G, Stokes M, Cousijn H, Woolrich M, Nobre AC (2015) Frontoparietal and Cingulo-opercular Networks Play Dissociable Roles in Control of Working Memory. Journal of Cognitive Neuroscience 27:2019–2034.

Walsh V, Cowey A (2000) Transcranial magnetic stimulation and cognitive neuroscience. Nat Rev Neurosci 1:73–79.

Wang X-J (2010) Neurophysiological and Computational Principles of Cortical Rhythms in Cognition. Physiological Reviews 90:1195–1268.

Yuste R (2015) From the neuron doctrine to neural networks. 16:487–497.

Ziemann U, Siebner HR (2015) Inter-subject and Inter- session Variability of Plasticity Induction by Non-invasive Brain Stimulation: Boon or Bane? Brain Stimulation 8:662–663.